PHILOSOPHICAL TRANSACTIONS OF THE ROYAL SOCIETY A MATHEMATICAL, PHYSICAL & ENGINEERING SCIENCES

Dynamo Action of Fluid Motions with Two-Dimensional Periodicity

G. O. Roberts

Phil. Trans. R. Soc. Lond. A 1972 **271**, 411-454
doi: 10.1098/rsta.1972.0015

DYNAMO ACTION OF FLUID MOTIONS WITH TWO-DIMENSIONAL PERIODICITY

By G. O. ROBERTS

Department of Engineering Science,
Northwestern University, Evanston, Illinois

(*Communicated by Sir Edward Bullard, F.R.S.—Received* 29 *September* 1970
—Revised 2 *August* 1971)

CONTENTS

Vol. 271. A. 1216. (Price £1.15; U.S. $3.00) 37 [Published 3 February 1972

In a previous paper it has been established that almost all spatially periodic motions of an infinite homogenous conducting fluid give magnetohydrodynamic dynamo action for almost all values of the magnetic diffusivity or resistivity λ. It was shown that there is a dynamo action if and only if for some real vector $\boldsymbol{j}$ there is a growing magnetic field solution of the form

$$\boldsymbol{B}(\boldsymbol{x}, t) = \boldsymbol{H}(\boldsymbol{x}) \exp(pt + \mathrm{i}\boldsymbol{j}\cdot\boldsymbol{x}),$$

where the complex vector function $\boldsymbol{H}(\boldsymbol{x})$ has the same periodicity as the motion. The complex growth rate p was studied in a first-order limit of small $\boldsymbol{j}$ to obtain the above result.

In this sequel the special case of spatially periodic motions with their three components functions of the two Cartesian coordinates y and z only is considered. The first-order method establishes dynamo action for only half, in a certain sense, of the motion-resistivity combinations.

It is shown that the two-dimensional spatially periodic motion

$$\boldsymbol{u} = (\cos y - \cos z, \sin z, \sin y)$$

is a first-order dynamo, at least for almost all resistivities. Three similar motions, which are not first-order dynamos for any resistivity, are also studied. It is proved that multiple-scale versions of all three can give growing magnetic fields for certain resistivities when terms of higher order in $\boldsymbol{j}$ are included. Heuristic descriptions of all four dynamo mechanisms are given.

A numerical method is described for determining the most rapidly growing magnetic field solution of the above form, and results for all four motions are presented, giving the growth rate $\mathrm{Re}\,p$ as a function of $\boldsymbol{j}$, for a range of resistivities λ down to about 10^{-2}. The first motion gives growing solutions for all resistivities in this range, the others give dynamo action only for resistivities below critical values near unity. The numerical and analytic results agree.

1. Introduction

The magnetohydrodynamic dynamo action of spatially periodic motions of an infinite homogenous conducting fluid has been studied previously (Roberts 1970*a*). This previous paper will be called part I, and its sections and equations referred to as, for example, § I, 4 and equation (I, 2.11). The main result was that almost all spatially periodic motions and motions periodic in space-time give dynamo action for almost all values of the magnetic diffusivity or resistivity λ. More precisely, for any given spatial periodicity, there is a set of infinitely differentiable motions, each of which will give dynamo action for all finite resistivities except for possibly a discrete set of resistivities with no non-zero point of accumulation. This set of motions is open with respect to the natural L_2 norm on the linear space of infinitely differentiable motions, and its closure includes the whole space.

The case of two-dimensional spatially periodic motions (with their three components spatially periodic functions of the Cartesian coordinates y and z only) is of particular interest in view of Cowling's theorem (1933) that magnetic fields independent of one Cartesian coordinate cannot be maintained by dynamo action. As shown below, this does not exclude the dynamo action of motions independent of one Cartesian coordinate. Further, such motions simplify the analytic and especially the numerical study of the dynamo action, and the dynamo mechanism can be understood more readily in heuristic terms of the 'freezing-in' of the field lines together with diffusion.

The application of the analysis of part I to these motions is summarized in §§ 2 and 3. It is shown again that there is dynamo action if and only if for some real vector $\boldsymbol{j}$ there is a magnetic field solution of the form

$$\boldsymbol{B}(\boldsymbol{x}, t) = \boldsymbol{H}(\boldsymbol{x}) \exp(pt + \mathrm{i}\boldsymbol{j}\cdot\boldsymbol{x}), \tag{1.1}$$

with $\mathrm{Re}\,p$ positive, where the vector function $\boldsymbol{H}(\boldsymbol{x})$ has the same periodicity as the motion. For small $\boldsymbol{j}$, there are solutions with $\mathrm{Re}\,p$ vanishing to zero order in $\boldsymbol{j}$ and positive to first order, if and only if two of the three eigenvalues of the symmetric part of a certain real 3×3 tensor α_{qr}, defined

for at least almost all resistivities, have the same sign. But in the two-dimensional case one eigenvalue is identically zero. It is shown that in a certain sense half of the motion-resistivity combinations are first-order dynamos and have growing solutions of the form (1.1) for sufficiently small $\boldsymbol{j}$ in all directions not in the y–z plane.

The particular two-dimensional spatially periodic motion

$$\boldsymbol{u} = (\cos y - \cos z, \sin z, \sin y)$$

is studied in § 5. Symmetry arguments introduced in § 4 are used to show that it is a first-order dynamo for all resistivities except possibly a discrete set with no non-zero point of accumulation.

Three further illustrative motions are introduced in § 6. The symmetry arguments establish that none is a first-order dynamo. A high-resistivity type of analysis is used in §§ 11 to 13 to show that multiple-scale versions of all three can give dynamo action for certain resistivities when terms of higher order in $\boldsymbol{j}$ are included.

Numerical results for the largest growth rate $\mathrm{Re}\, p$, as a function of $\boldsymbol{j}$, with $\boldsymbol{j}$ in the x-direction, are presented in § 9, for all four illustrative motions and for a range of resistivities down to about 10^{-2}. Accurate results could not be obtained for smaller resistivities with the computer storage and time available. The first motion gives growing field solutions for all resistivities in this range, the others give dynamo action only for resistivities below critical values near unity. The inverse iteration method used to find the fastest growing field solution is described, and questions of convergence and accuracy are discussed, in § 10.

A heuristic description of the four dynamo mechanisms in terms of the 'freezing-in' of magnetic field lines is given in § 7. The significance of the results, particularly in relation to further studies on the dynamo problem, is discussed in § 14.

Preliminary results for the last two motions have been published previously (Roberts 1969), without detailed description of the analytic and numerical methods employed, and prior to the discovery of the general result of part I. The presentation here is independent of the earlier one.

2. The motions and the magnetic field equations

It was shown in I, appendix A how the analysis of spatially periodic motions in §§ I, 2 and I, 3 can be extended to motions periodic in space-time. The extension to two-dimensional spatially periodic motions is simpler, and is therefore only summarized here.

A two-dimensional spatially periodic function is a function $f(y, z)$, independent of the Cartesian coordinate x, and satisfying the equations,

$$f(\boldsymbol{x}+\boldsymbol{l}_1) = f(\boldsymbol{x}+\boldsymbol{l}_2) = f(\boldsymbol{x}), \tag{2.1}$$

for all position vectors $\boldsymbol{x} = (x, y, z)$, where $\boldsymbol{l}_1 = (0, l_{1y}, l_{1z})$ and $\boldsymbol{l}_2 = (0, l_{2y}, l_{2z})$ are fixed independent vectors in the y–z plane. A function with the same periodicity as the motion $\boldsymbol{u}(y, z)$ under consideration will be called $\boldsymbol{u}$-periodic. The average and oscillatory parts of f are defined as

$$\left.\begin{aligned} f^{\mathrm{A}} &= \int_0^1 \mathrm{d}\xi_1 \int_0^1 \mathrm{d}\xi_2\, f(\boldsymbol{l}_1\xi_1 + \boldsymbol{l}_2\xi_2) \\ &= (1/\tau_2) \int_{\tau_2} f(y, z)\, \mathrm{d}y\, \mathrm{d}z, \end{aligned}\right\} \tag{2.2}$$

$$f' = f(\boldsymbol{x}) - f^{\mathrm{A}}, \tag{2.3}$$

where τ_2 is the area in the y–z plane defined by the first integral. Two-dimensional spatially periodic scalar and vector functions can be expressed in the Fourier series form

$$f(\boldsymbol{x}) = \sum_{\boldsymbol{k}\in K_2} \hat{f}(\boldsymbol{k}) \exp(\mathrm{i}\boldsymbol{k}\cdot\boldsymbol{x}), \tag{2.4}$$

where the set K_2 of three-dimensional vectors $\boldsymbol{k}$ is defined by

$$k_x = 0,$$

$$(k_y, k_z) = 2\pi L^{-1}(n_1, n_2), \tag{2.5}$$

where n_1 and n_2 are arbitary integers and

$$L = \begin{bmatrix} l_{1y} & l_{1z} \\ l_{2y} & l_{2z} \end{bmatrix}. \tag{2.6}$$

Equations (2.4) to (2.6) correspond to equations (I, 2.6) to (I, 2.9) in part I. From the definitions,

$$f^{\mathrm{A}} = \hat{f}(\boldsymbol{0}), \quad (f')^{\mathrm{A}} = 0, \quad (\nabla f)^{\mathrm{A}} = 0. \tag{2.7}$$

It may be shown as in § I, 2 that there is dynamo action, in the sense that with an initial field of finite total magnetic energy, this energy will grow indefinitely, if and only if there is a growing magnetic field solution of the form

$$\boldsymbol{B}(x, y, z, t) = \boldsymbol{H}(y, z) \exp(pt + \mathrm{i}\boldsymbol{j}\cdot\boldsymbol{x}), \tag{2.8}$$

where the complex vector function $\boldsymbol{H}(y, z)$ is $\boldsymbol{u}$-periodic, for some real vector $\boldsymbol{j}$ in the vector set J_2 with arbitrary x-component j_x and with y- and z- components given by

$$(j_y, j_z) = 2\pi L^{-1}(\nu_1, \nu_2),$$

for arbitrary ν_1, ν_2 satisfying $-\frac{1}{2} < \nu_i \leqslant \frac{1}{2}$, cf. equations (2.5) and (I, 2.22). Further, if dynamo action occurs, the results (I, 2.25) and (I, 2.29) for the asymptotic form of the growing magnetic field and the growing total magnetic energy as $t \to \infty$ apply without alteration.

The magnetic field equations for a fluid with uniform conductivity σ e.m.u. are

$$\nabla\cdot\boldsymbol{B} = 0, \tag{2.9}$$

$$\dot{\boldsymbol{B}} = \nabla\times(\boldsymbol{u}\times\boldsymbol{B}) + \lambda\nabla^2\boldsymbol{B}, \tag{2.10}$$

where λ is the resistivity or magnetic diffusivity $1/4\pi\sigma$. Attention is confined to incompressible fluids and to motions with zero average, so that

$$\nabla\cdot\boldsymbol{u} = 0, \quad \boldsymbol{u}^{\mathrm{A}} = 0, \tag{2.11}$$

and equation (2.10) can be written in the alternative form,

$$\dot{\boldsymbol{B}} = (\boldsymbol{B}\cdot\nabla)\boldsymbol{u} - (\boldsymbol{u}\cdot\nabla)\boldsymbol{B} + \lambda\nabla^2\boldsymbol{B}. \tag{2.12}$$

Substituting equation (2.8) into equations (2.9), (2.10) and (2.12) gives

$$(\nabla + \mathrm{i}\boldsymbol{j})\cdot\boldsymbol{H} = 0, \tag{2.13}$$

$$p\boldsymbol{H} = \mathscr{P}\boldsymbol{H}, \tag{2.14}$$

where $\mathscr{P}$ denotes the linear differential operator with the alternative forms, equivalent only for fields satisfying equation (2.13),

$$\mathscr{P}^{(1)}\boldsymbol{H} = (\nabla + \mathrm{i}\boldsymbol{j})\times(\boldsymbol{u}\times\boldsymbol{H}) + \lambda(\nabla + \mathrm{i}\boldsymbol{j})^2\boldsymbol{H}, \tag{2.15}$$

$$\mathscr{P}^{(2)}\boldsymbol{H} = (\boldsymbol{H}\cdot\nabla)\boldsymbol{u} - (\boldsymbol{u}\cdot\nabla + \mathrm{i}\boldsymbol{j})\boldsymbol{H} + \lambda(\nabla + \mathrm{i}\boldsymbol{j})^2\boldsymbol{H}. \tag{2.16}$$

The remaining sections are basically concerned with the eigenvalue problem defined by equations (2.13) to (2.16).

It should be noted that if the x-component of $\boldsymbol{j}$ is zero, the field $\boldsymbol{B}$ defined by equation (2.8) is independent of x, and must decay by Cowling's theorem (1933). But this theorem does not exclude the dynamo action of motions which are independent of x.

3. The first-order analysis and the general result

As in §I, 3, attention is now confined to small $\boldsymbol{j}$. The expansion of the eigensolution as

$$p = \sum_0^\infty p_n, \quad \boldsymbol{H}(\boldsymbol{x}) = \sum_0^\infty \boldsymbol{H}_n(\boldsymbol{x}),$$

where p_n and $\boldsymbol{H}_n(\boldsymbol{x})$ are explicitly of nth order in the components of $\boldsymbol{j}$, was justified in §I, appendix D. To zero order, the average of equation (2.14) with the alternative (2.15) gives

$$p_0 \boldsymbol{H}_0^{\mathrm{A}} = 0,$$

using the results (2.7). Attention is confined to eigensolutions with $\boldsymbol{H}_0^{\mathrm{A}}$ non-zero. To first order in the components of $\boldsymbol{j}$, the average of equation (2.14) becomes

$$p_1 \boldsymbol{H}_0^{\mathrm{A}} = \mathrm{i}\boldsymbol{j} \times (\boldsymbol{u} \times \boldsymbol{H}_0')^{\mathrm{A}}. \tag{3.1}$$

Now $(\boldsymbol{u} \times \boldsymbol{H}_0')^{\mathrm{A}}$ is uniquely determined by $\boldsymbol{H}_0^{\mathrm{A}}$, in the form

$$(\boldsymbol{u} \times \boldsymbol{H}_0')_q^{\mathrm{A}} = \alpha_{qr} \{\boldsymbol{H}_0^{\mathrm{A}}\}_r. \tag{3.2}$$

Here q and r take the values 1, 2 and 3 and the summation convention is implied. In equation (3.2), $\boldsymbol{H}_0'(\boldsymbol{x})$ is determined uniquely (at least for almost all resistivities λ) by the zero-order oscillatory part of equation (2.14)

$$\nabla \times (\boldsymbol{u} \times \boldsymbol{H}_0') + \lambda \nabla^2 \boldsymbol{H}_0' = -\nabla \times (\boldsymbol{u} \times \boldsymbol{H}_0^{\mathrm{A}}). \tag{3.3}$$

The real 3×3 tensor α_{qr} determined in equation (3.2) by the linear dependence of $\boldsymbol{H}_0'$ on $\boldsymbol{H}_0^{\mathrm{A}}$ is thus a function of the motion and resistivity only. It was shown in §I, 5 that if the restriction to real positive λ is removed, the tensor α_{qr} determined by equations (3.2) and (3.3) is an analytic function of λ, with non-zero poles but no other non-zero singularities.

Thus it is not necessary to study the first-order part $\boldsymbol{H}_1(\boldsymbol{x})$ of the eigenvector in obtaining the first-order part p_1 of the eigenvalue. Equations (3.1) and (3.2) are sufficient. The zero-order magnetic field solution,

$$\boldsymbol{B} = \boldsymbol{H}_0(\boldsymbol{x}),$$

is an exact steady $\boldsymbol{u}$-periodic solution of the magnetic field equation (2.10), and is obtained by setting $\boldsymbol{j}$ and p to zero in equation (2.8). It is this field solution which is perturbed in the analysis. Physically, equation (3.2) indicates the linear dependence of the average electromotive force $(\boldsymbol{u} \times \boldsymbol{B})^{\mathrm{A}}$ on the average magnetic field $\boldsymbol{B}^{\mathrm{A}}$ which is maintained at infinity.

The three-dimensional eigenvalue problem defined by equations (3.1) and (3.2) was studied in §I, 4. It was shown that there are $\boldsymbol{j}$-directions for which Re p_1 is positive, if and only if the symmetric part $\alpha_{\overline{qr}}$ of the real tensor α_{qr} has two non-zero eigenvalues with the same sign. Thus for dynamo action it is sufficient that the determinant of the symmetric part is non-zero, and this condition was used in §I, 5.

However, for the two-dimensional spatially periodic motions considered here, the first row and column of α_{qr} vanish. The first column vanishes since the right-hand side of equation (3.3) is zero when $\boldsymbol{H}_0^{\mathrm{A}}$ is in the x-direction, using equation (2.11). The first row vanishes since the x-component of $(\boldsymbol{u}\times\boldsymbol{H}_0')^{\mathrm{A}}$ in equation (3.2) is determined by the y- and z-components of $\boldsymbol{u}$ and $\boldsymbol{H}_0'$, which, using equation (2.11) and the equations,

$$\nabla\cdot\boldsymbol{H}_0' = 0, \quad (\boldsymbol{H}_0')^{\mathrm{A}} = 0,$$

are derivable from $\boldsymbol{u}$-periodic stream functions ψ_u and ψ_H. Thus the x-component, using equation (2.2), is

$$\begin{aligned}(\boldsymbol{u}\times\boldsymbol{H}_0')_x^{\mathrm{A}} &= \hat{\boldsymbol{x}}\cdot(\nabla\psi_u\times\nabla\psi_H)^{\mathrm{A}}\\ &= \hat{\boldsymbol{x}}\cdot\frac{1}{\tau_2}\int_{\tau_2}\nabla\times(\psi_u\nabla\psi_H)\,\mathrm{d}y\,\mathrm{d}z\\ &= 0;\end{aligned}$$

the integral vanishes when we invoke Gauss's theorem in two dimensions and the periodicity boundary condition.

Therefore the symmetric part $\alpha_{\overline{qr}}$ of the real tensor α_{qr} has one of its eigenvalues zero, corresponding to an eigenvector in the x-direction. The other two eigenvectors must lie in the y–z plane. If the corresponding two eigenvalues have the same sign, there are growing field solutions of the form (2.8) for sufficiently small $\boldsymbol{j}$ in all directions not in the y–z plane. If the two eigenvalues have opposite signs, or if more than one eigenvalue is zero, there is no dynamo action to first order in $\boldsymbol{j}$.

Equations (3.3) was solved in § 1, 5, with the general solution (I, 5.6),

$$\boldsymbol{H}_0' = (\lambda\mathscr{I}-\mathscr{Q})^{-1}(\nabla^2)^{-1}\{-\nabla\times(\boldsymbol{u}\times\boldsymbol{H}_0^{\mathrm{A}})\}, \tag{3.4}$$

valid if λ is not an eigenvalue of the compact operator $\mathscr{Q}$, on $\boldsymbol{u}$-periodic solenoidal vector functions with zero mean, defined by

$$\mathscr{Q}\boldsymbol{H}' = (\nabla^2)^{-1}\{-\nabla\times(\boldsymbol{u}\times\boldsymbol{H}')\}. \tag{3.5}$$

If λ is greater than the bound q of the bounded spectrum of $\mathscr{Q}$, equation (3.4) can be written as the convergent sum,

$$\boldsymbol{H}_0' = \sum_{n=0}^{\infty}\lambda^{-n-1}\mathscr{Q}^n(\nabla^2)^{-1}\{-\nabla\times(\boldsymbol{u}\times\boldsymbol{H}_0^{\mathrm{A}})\}, \tag{3.6}$$

cf. equation (I, 5.10). Thus, using the Fourier series forms corresponding to equation (2.4) for $\boldsymbol{u}$ and $\boldsymbol{H}_0'$, and using the corresponding form (I, 5.11) for the operator $\mathscr{Q}$, we can obtain $(\boldsymbol{u}\times\boldsymbol{H}_0')^{\mathrm{A}}$ in precisely the form (I, 5.12),

$$(\boldsymbol{u}\times\boldsymbol{H}_0')^{\mathrm{A}} = \sum_{l=2}^{\infty}\lambda^{1-l}\sum_{(l)}\boldsymbol{u}_l\times(\boldsymbol{\theta}_{l-1}\times(\boldsymbol{u}_{l-1}+\ldots\times(\boldsymbol{\theta}_1\times(\boldsymbol{u}_1\times\boldsymbol{H}_0^{\mathrm{A}}))\ldots)), \tag{3.7}$$

where $\sum_{(l)}$ denotes a sum over all ordered sets $\{\boldsymbol{k}_1,\boldsymbol{k}_2,\ldots,\boldsymbol{k}_l\}$ of l non-zero vectors in the set K_2 defined by equation (2.5), with zero sum and with non-zero partial sums

$$\boldsymbol{m}_i = \boldsymbol{k}_1+\boldsymbol{k}_2+\ldots+\boldsymbol{k}_i, \quad \text{and where} \quad \boldsymbol{u}_i = \hat{\boldsymbol{u}}(\boldsymbol{k}_i),\ \boldsymbol{\theta}_i = \mathrm{i}\boldsymbol{m}_i/\boldsymbol{m}_i^2.$$

Equation (3.7) gives α_{qr} as a power series in λ^{-1}, and can be rewritten as

$$\{(\boldsymbol{u}\times\boldsymbol{H}_0')^{\mathrm{A}}\}_q = \sum_{l=2}^{\infty}\frac{\alpha_{qr}^{(l)}}{\lambda^{l-1}}\{\boldsymbol{H}_0^{\mathrm{A}}\}_r \tag{3.8}$$

(cf. equation (3.2)). For all l values, $\alpha_{qr}^{(l)}$ has zeros in its first row and column. Childress (1967) has shown that $\alpha_{qr}^{(l)}$ is symmetric or antisymmetric according as l is even or odd. Further,

$$\alpha_{qr}^{(2)} = -4\sum_{(K_2)}\boldsymbol{v}\times\boldsymbol{w}\cdot\boldsymbol{k}(\boldsymbol{k}^2)^{-2}k_qk_r \tag{3.9}$$

(cf. equation (I, 5.18)); here $\hat{\boldsymbol{u}}(\boldsymbol{k}) = \boldsymbol{v} + \mathrm{i}\boldsymbol{w}$, and $\sum_{(K_2)}$ denotes a sum over non-zero vectors $\boldsymbol{k}$ in the set K_2 defined by equation (2.5) in which if $\boldsymbol{k}$ is included, $-\boldsymbol{k}$ is not.

The determinant $\alpha(\lambda, \boldsymbol{u})$ of the trailing 2×2 minor of $\alpha_{\bar{q}\bar{r}}$ is the product of the two eigenvalues which do not vanish identically. From above, there is dynamo action to first order in $\boldsymbol{j}$ if and only if $\alpha(\lambda, \boldsymbol{u})$ is positive. It is in this sense that half of the motion and resistivity combinations are first-order dynamos. The properties of $\alpha(\lambda, \boldsymbol{u})$ are discussed below, and the use of the word 'half' is defended.

The norm $\|\boldsymbol{u}\|$ on the linear space of infinitely differentiable motions of given two-dimensional spatial periodicity, defined by

$$\left.\begin{aligned} \|\boldsymbol{u}\| &= \frac{1}{\tau_2}\int_{\tau_2} |\boldsymbol{u}|^2 \mathrm{d}y\,\mathrm{d}z \\ &= \sum_{K_2} |\hat{\boldsymbol{u}}(\boldsymbol{k})|^2 \end{aligned}\right\} \tag{3.10}$$

(cf. equations (2.2) and (2.4)) is first introduced. Then from equation (3.4) and the definition (3.5) of the compact operator $\mathscr{Q}$, $\alpha(\lambda, \boldsymbol{u})$ is a continuous function of $(\lambda, \boldsymbol{u})$ wherever it is defined, and for fixed $\boldsymbol{u}$ is an analytic function of λ (with poles at the $\boldsymbol{u}$-dependent spectrum of $\mathscr{Q}$), real for real λ. Further, for $\lambda > q(\boldsymbol{u})$, $\alpha(\lambda, \boldsymbol{u})$ has the convergent power series expansion,

$$\alpha(\lambda, \boldsymbol{u}) = \sum_{l=2}^{\infty} \alpha^{(l)}(\boldsymbol{u})/\lambda^l, \tag{3.11}$$

cf. equation (3.8). Here $\alpha^{(l)} = 0$ for l odd, and

$$\alpha^{(2)}(\boldsymbol{u}) = |\alpha^{(2)}_{qr}|. \tag{3.12}$$

It can be shown easily from equation (3.9) that if $\alpha^{(2)}(\boldsymbol{u})$ is zero, there are motions arbitrarily close with $\alpha^{(2)}$ positive and negative. It can be shown with greater difficulty from equation (3.4) that if $\alpha(\lambda, \boldsymbol{u})$ is zero, there are motions arbitrarily near with α positive and negative, for the same value of λ. From the continuity property, it is clear that if $\alpha(\lambda, \boldsymbol{u})$ is non-zero for a given motion and positive resistivity, then it is non-zero, and has the same sign, for all sufficiently close motions and positive resistivities.

For any particular motion, it is only really practicable to obtain the first term $\alpha^{(2)}(\boldsymbol{u})$ of the above series. Thus a definite statement can only be made about whether it is a first-order dynamo for sufficiently large resistivities, and it would be hard to predict what sign changes in $\alpha(\lambda, \boldsymbol{u})$ might occur for lower resistivities. For the four illustrative motions studied below, symmetry arguments are used to obtain the form of the tensor α_{qr} for general resistivity. It is shown that $\alpha(\lambda, \boldsymbol{u})$ is positive for the first motion for almost all resistivities λ, while for the second motion $\alpha(\lambda, \boldsymbol{u})$ is identically negative. But such arguments can only be applied in special cases.

Clearly an analytic meaning cannot be attached to the statement that half the possible motion–resistivity combinations are first-order dynamos without the introduction of some sort of Lebesgue-type measure. It is reasonable, however, to state that half the motions with given spatial periodicity have a positive x-component at the origin. It appears equally reasonable to state that half have $\alpha^{(2)}$ positive and are first-order dynamos for sufficiently large λ, cf. equations (3.9) and (3.12). The full statement would be very unreasonable if the possibility remained that $\alpha(\lambda, \boldsymbol{u})$ is negative for all sufficiently small λ, but this possibility is excluded by the first illustrative motion. So the sign of $\alpha(\lambda, \boldsymbol{u})$ does divide the motion-resistivity combinations into two sets, neither having apparently any marked property making it 'bigger' than the other.

4. Symmetry arguments for the tensor α_{qr}

In this section the symmetry arguments used to establish the general form of the tensor α_{qr} for the four illustrative motions studied in this paper are described. The tensor is a function of the motion and of the resistivity λ. Coordinate transformations which leave the motion invariant are introduced for each motion, the corresponding tensor must then also be invariant under the transformation.

Consider the motion $\boldsymbol{u}(\boldsymbol{x})$, and the coordinate transformation given by

$$\boldsymbol{x}' = A\boldsymbol{x} + \boldsymbol{b}, \tag{4.1}$$

where $\boldsymbol{b}$ is fixed and A is a real orthogonal 3×3 matrix. Then in the new coordinates the same motion at the same position has components in the new coordinate directions given by

$$\boldsymbol{u}' = A\boldsymbol{u}. \tag{4.2}$$

This equation determines $\boldsymbol{u}'$ as a function of $\boldsymbol{x}$; equation (4.1) can then be used to find $\boldsymbol{u}'(\boldsymbol{x}')$. If $\boldsymbol{u}'(\boldsymbol{x}')$ has the same functional form as $\boldsymbol{u}(\boldsymbol{x})$, then the tensor α_{qr} must be invariant under the transformation. The transformed tensor is given by

$$\alpha'_{qr} = A_{qs} A_{rt} \alpha_{st}, \tag{4.3}$$

and the invariance implies that

$$\alpha'_{qr} = \alpha_{qr}. \tag{4.4}$$

The foregoing arguments must be changed slightly when coordinate reflexions are allowed. For pure rotations,

$$\det(A) = 1,$$

while for reflexions,

$$\det(A) = -1.$$

If reflexions are allowed, pure vectors and pure tensors transform according to equations (4.2) and (4.3) respectively, while pseudo-vectors and pseudo-tensors transform according to equations (4.2) and (4.3) with a sign change for reflexions. The alternating tensor ϵ_{qrs} is a pseudo-tensor. Now $\boldsymbol{u}$ is a pure vector; the cross-product in equation (3.2) then implies that α_{qr} is a pseudo-tensor, and a sign change must be included in equation (4.3) for reflexions.

5. The main illustrative motion

The first two-dimensional spatially periodic motion proposed as an example is the motion,

$$\boldsymbol{u} = (\cos y - \cos z, \sin z, \sin y). \tag{5.1}$$

This motion was chosen to make $\alpha^{(2)}$ positive, as defined by equations (3.9) and (3.12). In the equation for $\boldsymbol{u}(\boldsymbol{x})$ corresponding to equation (2.4),

$$\hat{\boldsymbol{u}}(0, 1, 0) = \tfrac{1}{2}(1, 0, -\mathrm{i}),$$

$$\hat{\boldsymbol{u}}(0, 0, 1) = \tfrac{1}{2}(-1, -\mathrm{i}, 0).$$

Substituting in equation (3.9),

$$\alpha^{(2)}_{qr} = \begin{bmatrix} 0 & 0 & 0 \\ 0 & -1 & 0 \\ 0 & 0 & -1 \end{bmatrix}, \tag{5.2}$$

and $\alpha^{(2)} = 1$. Thus the motion gives dynamo action at least for all sufficiently large resistivities.

The symmetry arguments described in § 4 can be used to show that this motion is a first-order dynamo for almost all resistivities λ. Consider the coordinate rotation given by

$$x' = -x, \quad y' = \pi - y, \quad z' = \pi + z, \tag{5.3}$$

cf. equation (4.1). Then, from equation (4.2),

$$\begin{aligned} u' &= (-\cos y + \cos z, \ -\sin z, \sin y) \\ &= (\cos y' - \cos z', \sin z', \sin y'), \end{aligned}$$

and the form of the motion is invariant. Suppose

$$\alpha_{rs} = \begin{bmatrix} 0 & 0 & 0 \\ 0 & a_1 & a_2 \\ 0 & a_3 & a_4 \end{bmatrix},$$

where a_1, a_2, a_3 and a_4 are analytic functions of λ, defined for almost all values of λ, and are real for real λ. Then substituting in equations (4.3) and (4.4), we have

$$\begin{bmatrix} 0 & 0 & 0 \\ 0 & a_1 & -a_2 \\ 0 & -a_3 & a_4 \end{bmatrix} = \begin{bmatrix} 0 & 0 & 0 \\ 0 & a_1 & a_2 \\ 0 & a_3 & a_4 \end{bmatrix},$$

and a_2 and a_3 vanish. Consider further the coordinate rotation given by

$$x' = x, \quad y' = \pi + z, \quad z' = \pi - y. \tag{5.4}$$

Then

$$\begin{aligned} u' &= (\cos y - \cos z, \sin y, \ -\sin z) \\ &= (\cos y' - \cos z', \sin z', \sin y'), \end{aligned}$$

and the form of the motion is invariant. Substituting in equation (4.4), we have

$$\begin{bmatrix} 0 & 0 & 0 \\ 0 & a_4 & 0 \\ 0 & 0 & a_1 \end{bmatrix} = \begin{bmatrix} 0 & 0 & 0 \\ 0 & a_1 & 0 \\ 0 & 0 & a_4 \end{bmatrix} = \begin{bmatrix} 0 & 0 & 0 \\ 0 & a & 0 \\ 0 & 0 & a \end{bmatrix}, \tag{5.5}$$

where $a(\lambda)$ is a real analytic function of λ, and is non-zero for sufficiently large λ from equation (5.2). Therefore $a(\lambda)$ cannot vanish identically except on a set of discrete λ values, at most denumerable and with no non-zero point of accumulation. So the determinant α is positive, and the motion is a first-order dynamo in the sense of § 3, for almost all resistivities.

It is also a Beltrami motion, with $\nabla \times \boldsymbol{u} = \boldsymbol{u}$. Thus it is a dynamically possible steady motion of an inviscid incompressible fluid with zero Lorentz force, since the equation for steady motion,

$$\rho(\boldsymbol{u} \cdot \nabla)\boldsymbol{u} = -\nabla p,$$

can be written as

$$\boldsymbol{u} \times (\nabla \times \boldsymbol{u}) = \nabla(p/\rho + \tfrac{1}{2}\boldsymbol{u}^2),$$

and this has the solution $p = p_0 - \frac{1}{2}\rho \boldsymbol{u}^2$ if the left-hand side vanishes.

In figure 1 the stream lines for the components of the motion in the y–z plane are shown, together with the sign of the x-component in the different regions of the y–z plane. It should be noted that the stream function $\cos y - \cos z$ for the components in the y–z plane is precisely the x-component of the motion, thus the stream lines are also lines of constant speed in the x-direction. Individual fluid particles therefore move at constant speed in the x-direction, while moving round the stream lines indicated.

A heuristic description of the dynamo mechanism for this motion is given in §7. Numerical results, giving the growth rate, for $\boldsymbol{j}$ in the x-direction, as a function of λ and j, are presented in §9.

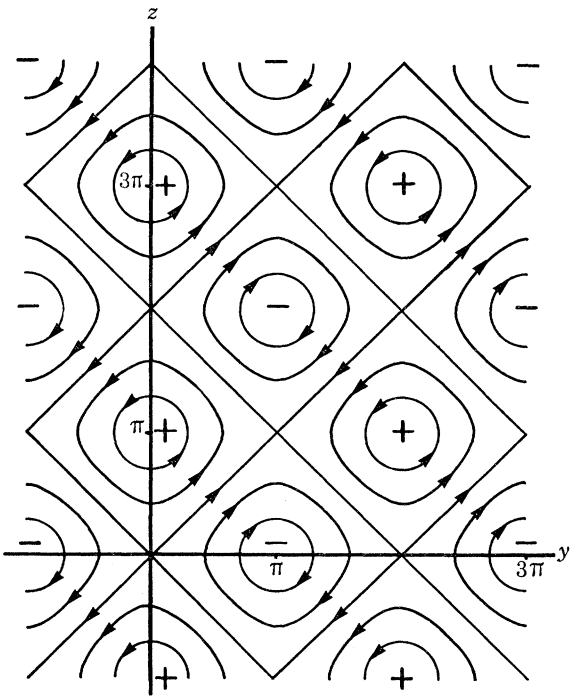

FIGURE 1. The sign of the x-component and the stream lines for the y- and z-components of the first motion given by $\boldsymbol{u} = (\cos y - \cos z, \sin z, \sin y)$.

6. THREE ADDITIONAL ILLUSTRATIVE MOTIONS

The three further motions introduced in this section are the following:

$$\boldsymbol{u} = (\cos y + \cos z, \sin z, \sin y), \tag{6.1}$$

$$\boldsymbol{u} = (2\cos y \cos z, \sin z, \sin y), \tag{6.2}$$

$$\boldsymbol{u} = (\sin(y+z), \sin 2z, \sin 2y). \tag{6.3}$$

The third and fourth motions were chosen on the basis of the heuristic arguments described in §7. The process of thought that led to these choices is described in detail in the paper presented in 1967 and published two years later (Roberts 1969). They were unfortunate choices in that for the fourth motion the tensor α_{qr} is identically zero, while for the third it is identically antisymmetric. The second illustrative motion was chosen to make $\alpha^{(2)}$ negative in the sum (3.11); in fact α is identically negative for this motion. So between them these three additional motions cover the main possibilities for motions which are not first-order dynamos.

The second motion is described in figure 2. Individual fluid particles move backwards and forwards in the x-direction while going round and round the stream lines; their net motion in the x-direction is zero from the symmetry. So each particle moves round a closed path. The third motion is shown in figure 3. For this motion some fluid particles while going round their stream lines move steadily in the negative x-direction, others move in alternate x-directions, with a net motion in either. The fourth motion is shown in figure 4; here each fluid particle in moving round its stream line is either always in a region of positive u_x or always in a region of negative u_x.

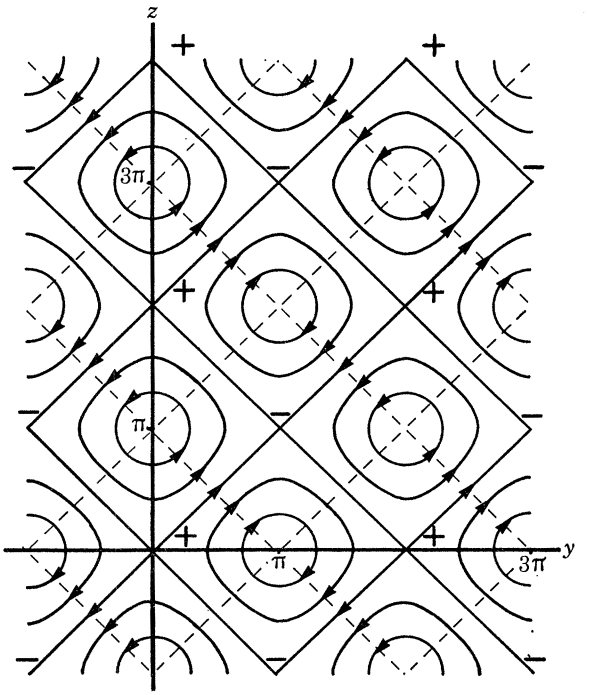

FIGURE 2. The second motion $\boldsymbol{u} = (\cos y + \cos z, \sin z, \sin y)$, with the sign of the x-component indicated.

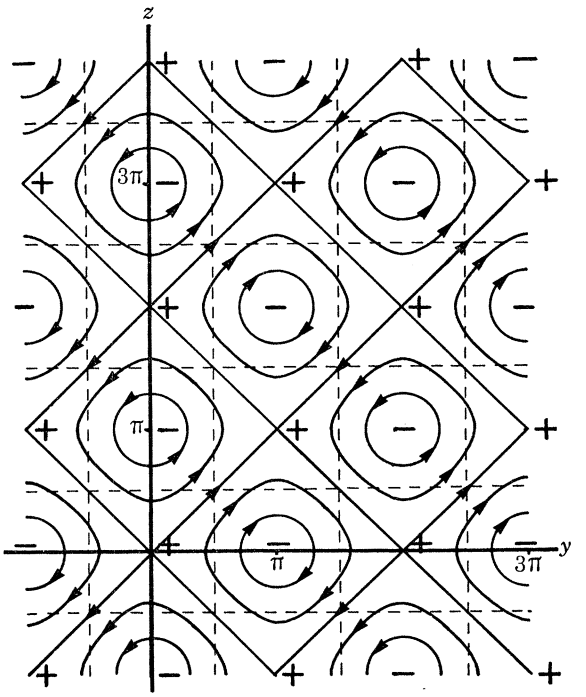

FIGURE 3. The third motion $\boldsymbol{u} = (2 \cos y \cos z, \sin z, \sin y)$, with the sign of the x-component indicated.

PHILOSOPHICAL TRANSACTIONS OF THE ROYAL SOCIETY A MATHEMATICAL, PHYSICAL & ENGINEERING SCIENCES

The shapes of the tensors α_{qr} for these three motions are given in table 2 on page 428. They are derived by using the symmetry arguments of § 4, with coordinate transformations similar to the transformations (5.3) and (5.4) used for the first motion. Full details are given in the second part of the author's dissertation, of which this paper is a shortened version (Roberts 1970*b*, pp. 102–105). It may be seen from table 2 that none of these three motions are first-order dynamos in the sense of § 3, for any resistivity λ, since the determinant α of the symmetric part of the trailing minor of the tensor α_{qr} is negative for the second motion and zero for the third and fourth motions.

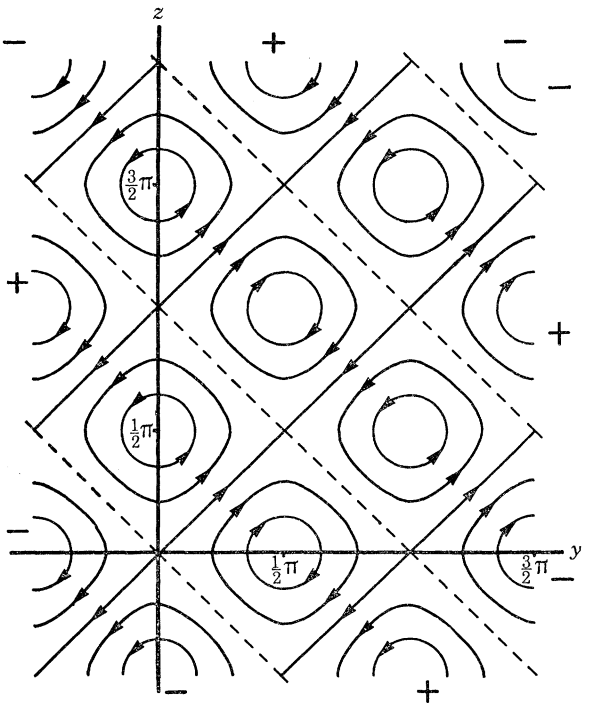

FIGURE 4. The fourth motion $\boldsymbol{u} = (\sin(y+z), \sin y, \sin z)$, with the sign of the x-component and the lines where it vanishes shown.

The numerical results presented in § 9 establish that all three motions act as dynamos for sufficiently small resistivities, when effects of second order and higher orders in the components of $\boldsymbol{j}$ are included. A heuristic description of the dynamo mechanisms is given in § 7.

It has not been found possible to prove analytically that these three motions can act as dynamos. Resistivities sufficiently high to make analysis practicable exclude dynamo action. The multiple-scale versions

$$\boldsymbol{u} = (U\cos ky + U\cos lz,\ V\sin lz,\ W\sin ky), \tag{6.4}$$

$$\boldsymbol{u} = (2U\cos ky\cos lz,\ V\sin lz,\ W\sin ky), \tag{6.5}$$

$$\boldsymbol{u} = (U\sin(ky+lz),\ V\sin 2lz,\ W\sin 2ky), \tag{6.6}$$

of the motions (6.1), (6.2) and (6.3) are therefore introduced. It is established in §§ 11 to 13 that for suitable values of the relevant parameters all three can give dynamo action, although they are not first-order dynamos. The value of these analytic results is in confirming the accuracy of the computer programs (cf. § 10 and appendix C) and in clarifying the dynamo mechanisms which operate for the single-scale motions.

7. Heuristic description of the four dynamo mechanisms

For motions with two-dimensional periodicity it is possible to get a physical picture of the dynamo mechanism in terms of the 'freezing-in' of field lines and subsequent diffusion. The field equation (2.12) can be written in the form,

$$\mathrm{D}\boldsymbol{B}/\mathrm{D}t = (\boldsymbol{B}\cdot\nabla)\boldsymbol{u} + \lambda\nabla^2\boldsymbol{B}, \tag{7.1}$$

where $\mathrm{D}/\mathrm{D}t$ denotes the material derivative $\partial/\partial t + (\boldsymbol{u}\cdot\nabla)$. For zero resistivity λ, the magnetic field lines behave precisely as if they were frozen to the fluid elements. If the magnetic field at a point at a given instant is parallel to an infinitesimal fluid element $\mathrm{d}\boldsymbol{s}$, then at any subsequent time the field at the element's instantaneous position will still be parallel to the element and will have increased in proportion to the length of the element. This is because the equation for the variation of $\mathrm{d}\boldsymbol{s}$ is clearly

$$\mathrm{D}(\mathrm{d}\boldsymbol{s})/\mathrm{D}t = (\mathrm{d}\boldsymbol{s}\cdot\nabla)\boldsymbol{u} \tag{7.2}$$

(cf. equation (7.1)). For finite resistivity λ, the magnetic diffusion tends to smooth the magnetic field out and keep the distortion of the field lines by the fluid motion from growing indefinitely.

The dynamo mechanism for the first motion (5.1) can be described in terms of figure 1. It may be seen that whenever a field line in the y–z plane is lifted upwards by the x-component of the motion it is twisted counter-clockwise; wherever it is moved downwards by the x-component it is twisted clockwise. Consider the initial field

$$\boldsymbol{B} = (0, \cos jx, 0),$$

with field lines in the positive y-direction near $jx = 0$, and in the negative y-direction near $jx = \pi$. After a time $1/\lambda$ (the diffusion time-scale) this field is distorted by the motion in such a way that the field lines near $jx = \frac{1}{2}\pi$ tend to be in the z-direction. The lines initially near $jx = 0$ are twisted anticlockwise; those initially near $jx = \pi$ are twisted clockwise. Thus the distortion of the field $(0, \cos jx, 0)$ generates a mean field which is a multiple of $(0, 0, \sin jx)$. Similarly, the distortion of an initial field $(0, 0, \sin jx)$ generates an additional mean field of the form $(0, \cos jx, 0)$. So the distortion of the initial field

$$(0, \cos jx, \sin jx)$$

generates an additional mean field of the same form, which serves to regenerate and amplify the initial field. The field pattern therefore remains stationary while the field amplitude grows steadily.

The dynamo mechanism for the second motion (6.1) can be described directly in terms of figure 2. It may be seen that whenever a field line initially in the direction $(0, 1, 1)$ is lifted by the x-component of the motion, it is stretched by the y- and z-components; whenever it is lowered it is contracted. For field lines initially in the $(0, 1, -1)$ direction the reverse is true. Thus the distortion of the initial field,

$$\boldsymbol{B} = (0, 1, \pm 1)\cos jx,$$

generates an additional mean field of the form,

$$\boldsymbol{B} = \pm\,(0, c, \pm c)\sin jx,$$

c being a positive constant. So two growing field solutions can be expected, with mean fields in the directions $(0, 1, 1)$ and $(0, 1, -1)$, and with the field pattern moving respectively in the positive and negative x-directions as the magnetic field grows.

An alternative heuristic explanation makes the relation of this motion to the first motion more clear. For both motions, from figures 1 and 2, wherever field lines initially in the y-direction are lifted up, they are twisted anticlockwise to go in the positive z-direction; wherever they are lowered the opposite is true. Thus the distortion of the field,

$$\boldsymbol{B} = (0, \cos jx, 0),$$

generates an additional mean field which is a multiple of the vector $(0, 0, \sin jx)$. This effect is the same for both motions because as functions of y, both motions are the same. But when field lines

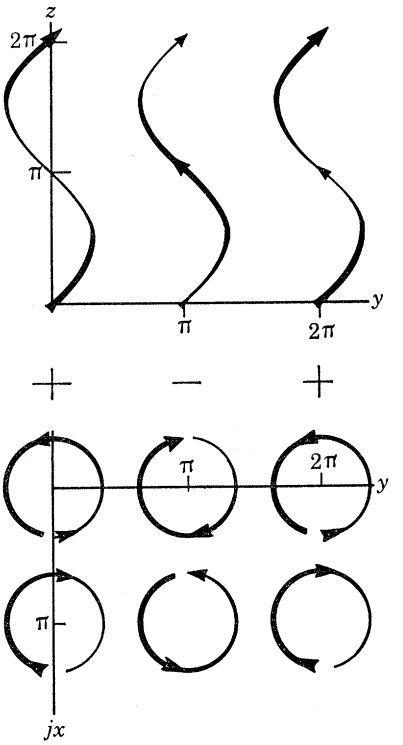

FIGURE 5. The dynamo mechanism for the third motion. The thickness of the field lines denotes closeness to the reader. Field lines in the z-direction are distorted into the indicated spirals. The reinforcement of the y-components at $jx = \frac{1}{2}\pi$ and the sign of the shear rate $\mathrm{d}u_z/\mathrm{d}y$ are shown.

initially in the z-direction are lifted up, they are twisted into the y-direction for the second motion but into the negative y-direction for the first. This is a consequence of the change in sign of the part of u_x which is a function of z. So the distortion of the field,

$$\boldsymbol{B} = (0, 0, \cos jx),$$

generates an additional mean field which is a positive multiple of the vector $(0, \sin jx, 0)$ for the second motion, and a negative multiple for the first. This makes it clear why the first motion is a more efficient dynamo and why the field pattern moves for the second motion as the field grows.

The dynamo mechanism for the third motion (6.2) is illustrated in figure 5. Field lines initially in the z-direction are distorted by the motion into the indicated spirals. With the initial field,

$$\boldsymbol{B} = (0, 0, \cos jx), \tag{7.3}$$

the field lines alternate in direction for jx equal to successive multiples of π. The figure illustrates in the (x, y) diagram the reinforcement of the y-components of the distorted field at each value of y

for values of jx near odd multiples of $\frac{1}{2}\pi$. Clearly the average of the distorted field with respect to z has a y-component of the form,

$$B_y = \sin jx \cos y.$$

This field is distorted by the z-component $\sin y$ of the motion to produce an additional mean field of the form,

$$\boldsymbol{B} = (0, 0, \sin jx). \tag{7.4}$$

In the figure it can be seen that the reinforced y-component at $jx = \frac{1}{2}\pi$ always has the same sign as the shear rate du_z/dy. Thus the product is positive, and the distortion of the y-component gives a

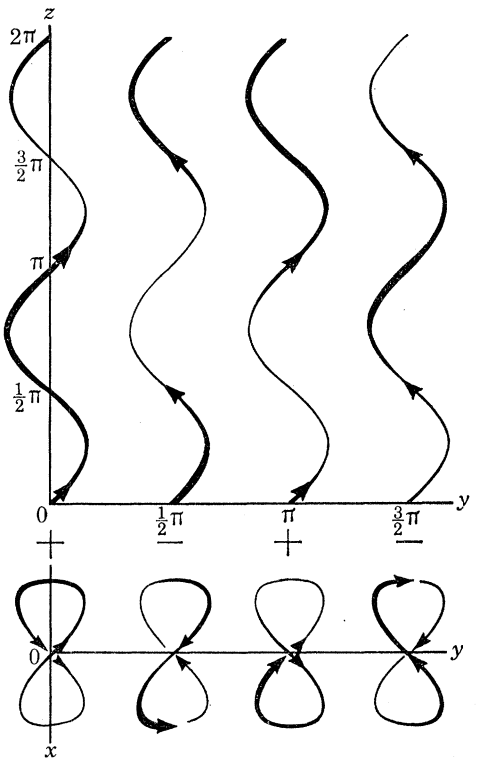

FIGURE 6. The dynamo mechanism for the fourth motion. The thickness of the field lines indicates closeness to the reader. Field lines in the z-direction are distorted into the double spirals shown. The reinforcement of the y-components and the sign of the shear rate du_z/dy are indicated.

field in the positive z-direction, in agreement with equation (7.4). Equations (7.3) and (7.4) together imply that the field pattern moves in the positive x-direction as the field grows. The symmetry of the motion (6.2) between the y- and z-directions establishes that there is a corresponding growing field solution with the mean field in the y-direction, with the field pattern also moving steadily in the positive x-direction.

The dynamo mechanism for the fourth motion (6.3) is illustrated in figure 6. Field lines initially in the z-direction are distorted into the indicated double spirals, and where these distorted lines pass through the original position, the y-components reinforce. Clearly, with an initial field of the form (7.3), the average of the distorted field with respect to z has a y-component of the form

$$B_y = \cos jx \cos 2y.$$

This component is distorted by the z-component $\sin 2y$ of the motion to generate an additional mean field component of the form (7.3), so that the field grows steadily with the field pattern

remaining stationary. It may be seen in the figure that the reinforcing y-components have the same sign as the shear rate $\mathrm{d}u_z/\mathrm{d}y$ near $x = 0$, so that the interaction regenerates the initial field in the z-direction. Further, the symmetry of the motion (6.3) between the y- and z-directions again establishes that there is a corresponding growing field solution with the mean field in the y-direction.

These heuristic arguments are confirmed by the numerical results reported in §§ 9 and 10. They are summarized in table 1. The distortion of initial fields $(0, \cos jx, 0)$ and $(0, 0, \cos jx)$

TABLE 1. SUMMARY OF THE FOUR MECHANISMS

motion ...		I(5.1)	II(6.1)	III(6.2)	IV(6.3)
illustrative diagrams		figure 1	figure 2	figures 3, 5	figures 4, 6
initial field		direction and phase of mean of generated field			
component sinusoidal in jx	B_y	B_z ahead	B_z ahead	B_y ahead	B_y same
	B_z	B_y behind	B_y ahead	B_z ahead	B_z same
alternatives for the mean of the growing field		$(0, \cos jx, \sin jx)$	$(0, 1, 1)\cos jx$ $(0, 1, -1)\cos jx$	$(0, \cos jx, 0)$ $(0, 0, \cos jx)$	$(0, \cos jx, 0)$ $(0, 0, \cos jx)$
motion in x-direction of the growing magnetic field pattern		stationary	positive negative	positive	stationary

generates fields with their means with respect to y and z having additional parts in the y- or z-direction, possibly advanced or retarded in phase, as indicated in the table and derived above. Thus the distortion of the field $(0, \cos jx, 0)$ by the first motion generates the additional mean field $(0, 0, \sin jx)$, which is ahead in phase. These results determine the indicated alternatives for the mean of the growing field, so that the additional mean field is a reinforcement. The phases determine any motion in the x-direction of the growing magnetic field pattern.

8. THE FOURIER-ANALYSED EQUATIONS

In this section the eigenvalue problem (2.14) is expressed in its Fourier series form. This form is required for the numerical work described in §§ 9 and 10, and for the analysis of the multiple-scale motions in §§ 11 to 13. For convenience of description only, the multiple-scale version,

$$\boldsymbol{u} = (U\cos ky - U\cos lz,\ V\sin lz,\ W\sin ky), \tag{8.1}$$

of the first illustrative motion (5.1) is introduced.

Attention will be confined to vectors $\boldsymbol{j}$ in the x-direction in the numerical work and in the study of the multiple-scale motions. This is not strictly necessary, but it simplifies the expressions and the analysis, which are complicated enough anyway. Thus

$$\boldsymbol{j} = j\hat{\boldsymbol{x}}, \tag{8.2}$$

and the operator $(\boldsymbol{j}\cdot\nabla)$ on $\boldsymbol{u}$-periodic functions is zero. Equation (2.14) with the alternative form (2.16) used for the operator $\mathscr{P}$, then reduces to the equation,

$$p^*\boldsymbol{H} = -(\boldsymbol{u}\cdot\mathrm{i}\boldsymbol{j})\boldsymbol{H} - (\boldsymbol{u}\cdot\nabla)\boldsymbol{H} + (\boldsymbol{H}\cdot\nabla)\boldsymbol{u} + \lambda\nabla^2\boldsymbol{H}, \tag{8.3}$$

where

$$p^* = p + \lambda j^2. \tag{8.4}$$

The y- and z-components of equation (8.3) do not involve H_x, so it is sufficient to confine attention to these. Then H_x, as determined by equation (2.13) in the form,

$$ij\,H_x + \nabla\cdot\boldsymbol{H} = 0, \tag{8.5}$$

automatically satisfies the x-component of equation (8.3).

The equations are derived in terms of the multiple-scale forms (8.1) and (6.4) to (6.6) of the illustrative motions; the analysis will then include the special case $U = V = W = k = l = 1$, for which the motions reduce to the simple forms (5.1) and (6.1) to (6.3).

The changes of coordinates and of variables given by

$$\left.\begin{aligned} \eta &= ky, \quad \zeta = lz, \\ \boldsymbol{h} &= (f, g) \\ &= (kH_y, lH_z), \end{aligned}\right\} \tag{8.6}$$

$$\boldsymbol{u} = (Uv_x, Vv_y, Wv_z), \tag{8.7}$$

are now made. Here $\boldsymbol{v}(\eta, \zeta)$ has the same forms as the motions $\boldsymbol{u}(y, z)$ given by equations (5.1) and (6.1) to (6.3). The y- and z-components of equation (8.3) reduce to

$$\begin{aligned} p^*\boldsymbol{h} - (\lambda k^2)\frac{\partial^2\boldsymbol{h}}{\partial\eta^2} - (\lambda l^2)\frac{\partial^2\boldsymbol{h}}{\partial\zeta^2} \\ = -\mathrm{i}(Uj)v_x\boldsymbol{h} - (Vk)v_y\frac{\partial\boldsymbol{h}}{\partial\eta} - (Wl)v_z\frac{\partial\boldsymbol{h}}{\partial\zeta} + \left\{(Vk)g\frac{\partial v_y}{\partial\zeta},\ (Wl)f\frac{\partial v_z}{\partial\eta}\right\}. \end{aligned} \tag{8.8}$$

In this equation the quantities λk^2 and λl^2 are the inverse decay time-scales for the length scales in the y- and z-directions respectively, and Uj, Vk and Wl are the inverse convection time-scales for convection in the three coordinate directions. These quantities will be kept in this dimensional form so that the physical significance of the various terms is apparent.

Now $\boldsymbol{h}(\eta, \zeta)$ is written in the Fourier series form

$$\boldsymbol{h}(\eta, \zeta) = \Sigma\boldsymbol{h}_{m,n}\exp(\mathrm{i}m\eta + \mathrm{i}n\zeta), \tag{8.9}$$

where for the first three motions the sum is over all integers m and n, while for the fourth it is over all pairs with $m+n$ even, corresponding to the form of the motion (6.3). Then for the second, third and fourth motions, equation (8.8) gives

$$\begin{aligned} \{p^* + m^2(\lambda k^2) + n^2(\lambda l^2)\}\boldsymbol{h}_{m,n} \\ = -\tfrac{1}{2}\mathrm{i}(Uj)\{\boldsymbol{h}_{m+1,n} + \boldsymbol{h}_{m-1,n} + \boldsymbol{h}_{m,n+1} + \boldsymbol{h}_{m,n-1}\} \\ + \tfrac{1}{2}m(Vk)\{\boldsymbol{h}_{m,n+1} - \boldsymbol{h}_{m,n-1}\} + \tfrac{1}{2}n(Wl)\{\boldsymbol{h}_{m+1,n} - \boldsymbol{h}_{m-1,n}\} \\ + \{\tfrac{1}{2}(Vk)(g_{m,n+1} + g_{m,n-1}),\ \tfrac{1}{2}(Wl)(f_{m+1\,n} + f_{m-1\,n})\}, \end{aligned} \tag{8.10}$$

$$\begin{aligned} \{p^* + m^2(\lambda k^2) + n^2(\lambda l^2)\}\boldsymbol{h}_{m,n} \\ = -\tfrac{1}{2}\mathrm{i}(Uj)\{\boldsymbol{h}_{m+1,n+1} + \boldsymbol{h}_{m+1,n-1} + \boldsymbol{h}_{m-1,n+1} + \boldsymbol{h}_{m-1,n-1}\} \\ + \tfrac{1}{2}m(Vk)\{\boldsymbol{h}_{m,n+1} - \boldsymbol{h}_{m,n-1}\} + \tfrac{1}{2}n(Wl)\{\boldsymbol{h}_{m+1,n} - \boldsymbol{h}_{m-1,n}\} \\ + \{\tfrac{1}{2}(Vk)(g_{m,n+1} + g_{m,n-1}),\ \tfrac{1}{2}(Wl)(f_{m+1,n} + f_{m-1,n})\}, \end{aligned} \tag{8.11}$$

$$\{p^* + m^2(\lambda k^2) + n^2(\lambda l^2)\}\boldsymbol{h}_{m,n}$$
$$= \tfrac{1}{2}(Uj)\{\boldsymbol{h}_{m+1,n+1} - \boldsymbol{h}_{m-1,n-1}\}$$
$$+ \tfrac{1}{2}m(Vk)\{\boldsymbol{h}_{m,n+2} - \boldsymbol{h}_{m,n-2}\} + \tfrac{1}{2}n(Wl)\{\boldsymbol{h}_{m+2,n} - \boldsymbol{h}_{m-2,n}\}$$
$$+ \{(Vk)(g_{m,n+2} + g_{m,n-2}), (Wl)(f_{m+2,n} + f_{m-2,n})\}, \tag{8.12}$$

respectively. For the first motion (5.1), equation (8.8) becomes

$$\{p^* + \lambda(m^2 + n^2)\}\boldsymbol{h}_{m,n}$$
$$= -\tfrac{1}{2}ij(\boldsymbol{h}_{m+1,n} + \boldsymbol{h}_{m-1,n} - \boldsymbol{h}_{m,n+1} - \boldsymbol{h}_{m,n-1})$$
$$+ \tfrac{1}{2}m(\boldsymbol{h}_{m,n+1} - \boldsymbol{h}_{m,n-1}) + \tfrac{1}{2}n(\boldsymbol{h}_{m+1,n} - \boldsymbol{h}_{m-1,n})$$
$$+ \tfrac{1}{2}\{(g_{m,n+1} + g_{m,n-1}), (f_{m+1,n} + f_{m-1,n})\}, \tag{8.13}$$

and the corresponding equations for the second, third and fourth motions in their single-scale forms (6.1) to (6.3) can be obtained from equations (8.10) to (8.12) by setting U, V, W, k and l equal to unity. For each of the equations (8.10) to (8.13), the successive terms on the right-hand sides correspond to convection in the x, y and z directions, to the distortion of B_z into B_y, and to the distortion of B_y into B_z.

In obtaining the numerical results, the symmetry properties of the eigensolutions $\boldsymbol{h}_{m,n}$, indicated for the four single-scale motions in table 2, are used, to reduce the number of independent components. The rigorous derivation of these symmetry properties is difficult and tedious, and is postponed to appendix A.

TABLE 2. THE FOUR SINGLE-SCALE MOTIONS

motion ...	I	II	III	IV
trailing minor of α_{rs} shape of ϕ_{qr}	$\begin{bmatrix} a & 0 \\ 0 & a \end{bmatrix}$ $\begin{bmatrix} \kappa & \mu \\ -\mu & \kappa \end{bmatrix}$	$\begin{bmatrix} a & 0 \\ 0 & -a \end{bmatrix}$ $\begin{bmatrix} \kappa & \mu \\ \mu & \kappa \end{bmatrix}$	$\begin{bmatrix} 0 & b \\ -b & 0 \end{bmatrix}$ $\begin{bmatrix} \kappa & 0 \\ 0 & \kappa \end{bmatrix}$	$\begin{bmatrix} 0 & 0 \\ 0 & 0 \end{bmatrix}$ $\begin{bmatrix} \kappa & 0 \\ 0 & \kappa \end{bmatrix}$
coordinate transformations leaving motion invariant	$\begin{cases} x' = -x, \\ y' = \pi - y, \\ z' = \pi + z; \end{cases}$ $\begin{cases} x' = x, \\ y' = \pi + z, \\ z' = \pi - y \end{cases}$	$\begin{cases} x' = -x, \\ y' = \pi - y, \\ z' = \pi + z; \end{cases}$ $\begin{cases} x' = x, \\ y' = z, \\ z' = y \end{cases}$	$\begin{cases} x' = x, \\ y' = \pi - y, \\ z' = \pi + z; \end{cases}$ $\begin{cases} x' = x, \\ y' = z, \\ z' = y \end{cases}$	$\begin{cases} x' = -x, \\ y' = -y, \\ z' = -z; \end{cases}$ $\begin{cases} x' = x, \\ y' = z, \\ z' = y \end{cases}$
dominant eigenvalues	real	conjugate pairs	complex, repeated	real, repeated
operations on the eigenvectors giving new eigenvectors	$(R\boldsymbol{h})_{m,n} = \boldsymbol{h}_{-m,-n}$; $(T\boldsymbol{h})_{m,n} = (-1)^{m+n}$ $(-g_{-n,m}, f_{-n,m})$; and, corresponding to $\overline{p^*}$, $(\overline{Q}h)_{m,n} = (\overline{g_{n,m}}, \overline{f_{n,m}})$	$(R\boldsymbol{h})_{m,n} = \boldsymbol{h}_{-m,-n}$; $(Q\boldsymbol{h})_{m,n} = (g_{n,m}, f_{n,m})$; and, corresponding to $\overline{p^*}$, $(\overline{P}h)_{n,m} = (-1)^{m+n}$ $(\overline{f_{-m,n}}, -\overline{g_{-m,n}})$	$(R\boldsymbol{h})_{m,n} = \boldsymbol{h}_{-m,-n}$; $(Q\boldsymbol{h})_{m,n} = (g_{n,m}, f_{n,m})$; $(P\boldsymbol{h})_{m,n} = (-1)^{m+n}$ $(f_{-m,n}, -g_{-m,n})$	$(S\boldsymbol{h})_{m,n} = (-1)^m \boldsymbol{h}_{-m,-n}$; $(Q\boldsymbol{h})_{m,n} = (g_{n,m}, f_{n,m})$
properties of the operators	$T^2 = -R$, $T^4 = I$, $P_\omega = I + \omega T + \omega^2 T^2 + \omega^3 T^3$, where $\omega^4 = 1$, $(I - \omega T)P_\omega = 0$, $\overline{Q}^2 = I$, $\overline{Q}P_\omega = P_\omega \overline{Q}$	$\overline{P}^2 = Q^2 = R^2 = \mathrm{I}$, $R\overline{P} = \overline{P}R$, $RQ = QR$, $\overline{P}Q = -Q\overline{P}R$	$P^2 = Q^2 = R^2 = \mathrm{I}$, $RP = PR$, $RQ = QR$, $PQ = -QPR$	$Q^2 = S^2 = \mathrm{I}$, $QS = SQ$
can confine attention to eigenvectors invariant under the operations (only underlined options were studied)	$\begin{cases} \omega T \text{ in general}; \\ \omega T, \overline{Q} \text{ for real } p^*; \end{cases}$ where $\omega = -\mathrm{i}$ or $+\underline{\mathrm{i}}$ or ± 1.	$\underline{R, Q}$ $\begin{cases} -R, \pm \underline{Q}, \text{in general}; \\ -R, \pm Q, \overline{P} \text{ for real } p^*. \end{cases}$	either R, Q or R, P; $-R, \pm Q, \overline{P}$	S, Q; $-S, \overline{Q}$

9. Numerical results for the four motions

The eigenvalue equations for the four illustrative motions were presented in § 8 above, and the symmetry properties of the Fourier components are shown in table 2. The numerical method which was used for finding the eigenvalue p^* with the largest real part is described in § 10 and the accuracy of the programs is defended in appendix C. The results are presented here as curves giving the growth rate,

$$\mathrm{Re}\, p = \mathrm{Re}\, p^* - \lambda j^2, \tag{9.1}$$

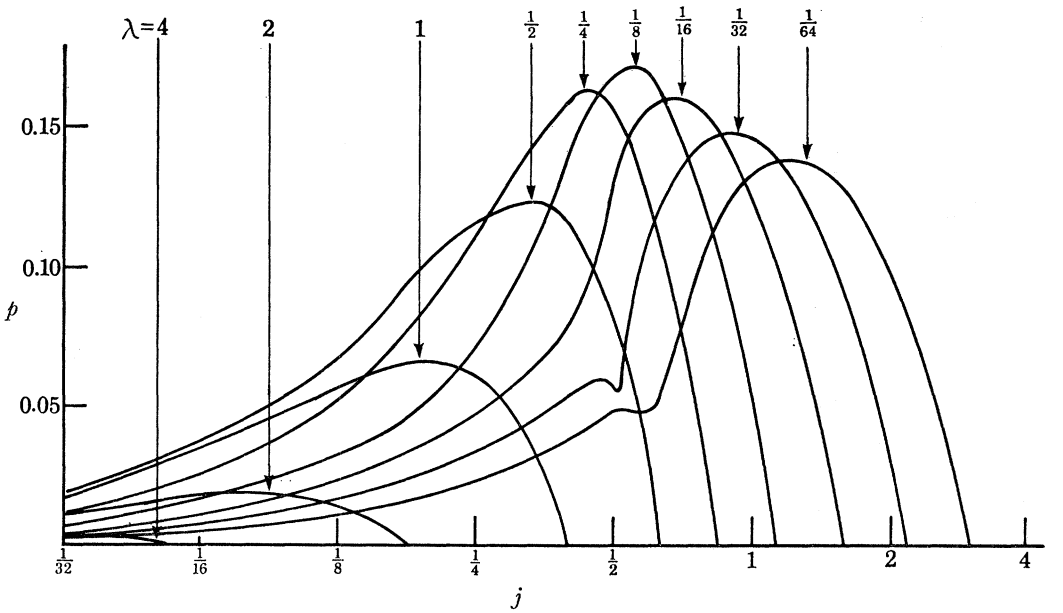

Figure 7. Numerical results giving the growth rate for the first motion for the indicated resistivities λ.

as a function of j, for resistivities λ equal to all powers of 2 down to $\frac{1}{32}$ or $\frac{1}{64}$. The results are as accurate as can be shown on a graph, i.e. 3 significant figures, except for the lowest resistivity indicated on each graph: the accuracy and convergence are discussed in § 10. A selection of the numerical results is given in table 4 on page 435.

The numerical results for the first motion (5.1) are given in figure 7. For the largest growth rate the eigenvalue was always real, as predicted by the heuristic argument in § 7. There is dynamo action for all resistivities λ considered. For fixed λ, there are field solutions with positive growth rate $\mathrm{Re}\, p$ for all values of j below a critical value, which increases as λ decreases and takes the remarkable value 3.0 for $\lambda = \frac{1}{64}$. Further, the growth rate tends to zero as j tends to zero, and for fixed λ has a maximum value. This peak growth rate increases to a maximum and then decreases, as λ decreases; the corresponding value of j continues to increase. The growth rate maximum is approximately given by

$$p = 0.173, \quad \text{for} \quad \lambda = \tfrac{1}{8}, \quad j = 0.55.$$

The kinks in the curves for $\lambda = \frac{1}{32}$ and $\lambda = \frac{1}{64}$ have naturally received considerable study, and the results are especially accurate in those regions. Using a very small j-interval, the successive eigenvalue differences vary continuously. The likely explanation for these kinks is that in a region in a λ, j plane for which there is nearly a degenerate eigenvalue, the two eigenvalues take the form

$$p = \chi \pm \sqrt{\xi} \tag{9.2}$$

(cf. the two roots of a quadratic equation). This result follows from the perturbation theory of non-Hermitian operators. Here χ and ξ are real functions of λ and j, and it appears that ξ takes small values near the point $\lambda = \frac{1}{32}, j = 0.5$, so that the derivative

$$\frac{\partial p}{\partial j} = \frac{\partial \chi}{\partial j} + \tfrac{1}{2}\xi^{-\frac{1}{2}}\frac{\partial \xi}{\partial j} \tag{9.3}$$

of the largest eigenvalue is large there.

The results for values of j smaller than those indicated confirm the results of § 3 and the result of § 5 that this motion is a first-order dynamo for at least almost all resistivities. The tensor α_{qr} takes the form (5.5),

$$\alpha_{qr} = \begin{bmatrix} 0 & 0 & 0 \\ 0 & a & 0 \\ 0 & 0 & a \end{bmatrix},$$

TABLE 3. NUMERICAL RESULTS FOR THE FUNCTION $\alpha(\lambda)$

λ ...	50	8	4	2	1	$\frac{1}{2}$
$\lvert\alpha\rvert$	0.0198	0.124	0.242	0.444	0.655	0.620
$\lambda\lvert\alpha\rvert$	0.99	0.99	0.97	0.89	0.66	0.31
λ	$\frac{1}{2}$	$\frac{1}{4}$	$\frac{1}{8}$	$\frac{1}{16}$	$\frac{1}{32}$	$\frac{1}{64}$
$\lvert\alpha\rvert$	0.620	0.394	0.266	0.187	0.131	0.085

where $a(\lambda)$ is analytic and real for real λ. The exception resistivities are the zeros and poles of $a(\lambda)$. It was shown in § 3 that

$$p \sim |a(\lambda)|j \quad \text{as} \quad j \to 0, \tag{9.4}$$

using the results of § I, 4. The numerical work confirms this, and results for $|a(\lambda)|$ are shown in table 3. These confirm the result (5.2) that

$$a(\lambda) = -\lambda^{-1} + O(\lambda^{-3}), \tag{9.5}$$

and indicate that $a(\lambda)$ has no zeros or poles in the resistivity range considered.

The results for the second, third and fourth motions, in their single-scale forms (6.1) to (6.3), are shown in figures 8 to 10. There is dynamo action for all resistivities λ below critical values, respectively

$$\lambda = 0.55, \quad \lambda = 0.8, \quad \lambda = 0.2,$$

for the three motions. For fixed λ below the critical values, there is a growing field solution for all j below a critical value. The growth rates are smaller than for the first motion; the approximate peak values and the corresponding λ and j values are respectively,

$$\begin{aligned} \operatorname{Re} p &= 0.025, \quad \lambda = \tfrac{1}{8}, \quad j = 0.28, \\ \operatorname{Re} p &= 0.09, \quad \lambda = \tfrac{1}{8}, \quad j = 0.27, \\ p &= 0.10, \quad \lambda = \tfrac{1}{64}, \quad j = 1.6. \end{aligned}$$

The shapes of the tensor α_{qr}, presented in table 2 on page 428, establish that none of the three motions is a first-order dynamo for any resistivity. This is confirmed by the numerical results, which show that for fixed λ,

$$\operatorname{Re} p \sim e(\lambda)j^2 \quad \text{as} \quad j \to 0,$$

where $e(\lambda)$ can be positive or negative.

For the fourth motion the eigenvalues found were real. For the second they occurred in conjugate pairs, in agreement with the symmetry results indicated in table 2, while for the third motion $\operatorname{Im} p$ was always negative for growing field solutions. The form of the exponential term,

$$\exp(pt + \mathrm{i}\boldsymbol{j}\cdot\boldsymbol{x}),$$

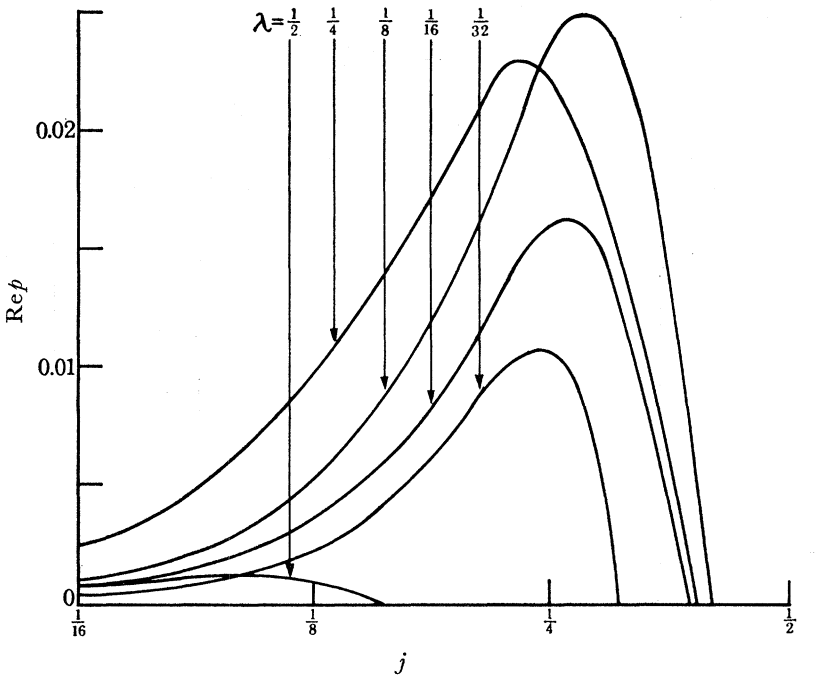

FIGURE 8. Numerical results giving the growth rate for the second motion for the indicated resistivities λ.

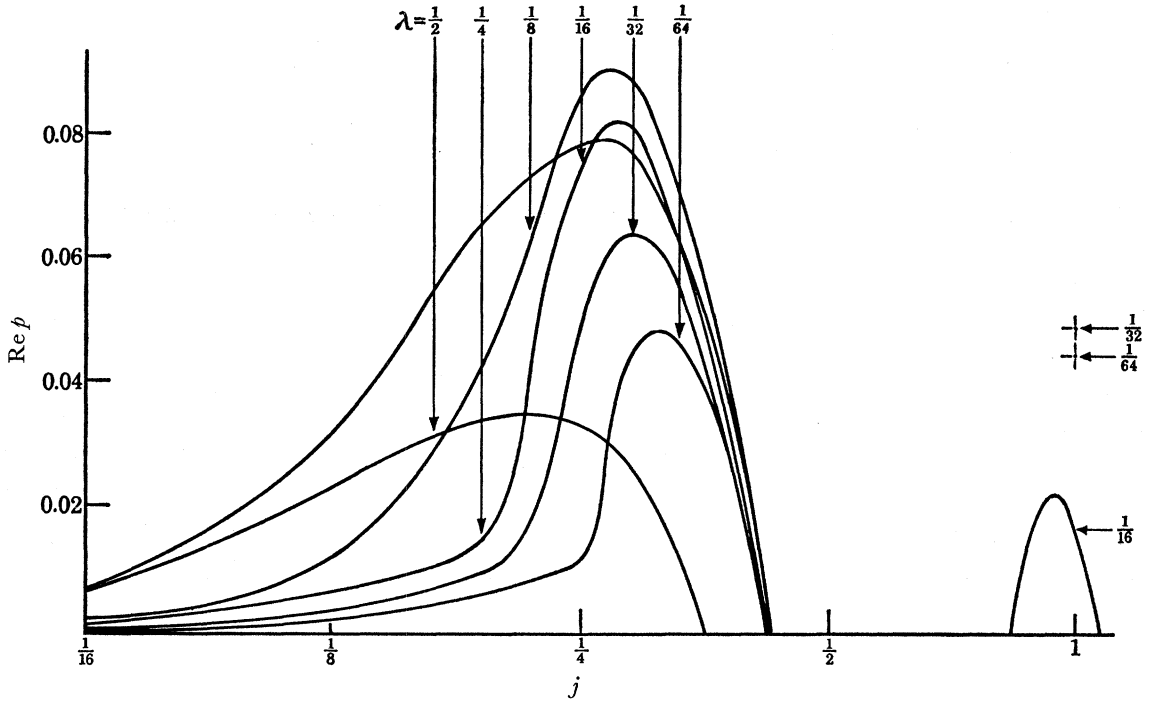

FIGURE 9. Numerical results giving the growth rate for the third motion, for the indicated resistivities λ.

PHILOSOPHICAL TRANSACTIONS OF THE ROYAL SOCIETY A MATHEMATICAL, PHYSICAL & ENGINEERING SCIENCES

in equation (2.8), indicates that for j in the x-direction the growing or decaying field pattern moves in the x-direction with phase velocity

$$-\operatorname{Im} p/j.$$

From the numerical results for the second motion, this phase velocity is in the positive or negative x-direction for growing fields satisfying the symmetry condition in table 2 with the positive or negative alternative respectively; the amplitude is between 1.5 and 2.0. For the third motion,

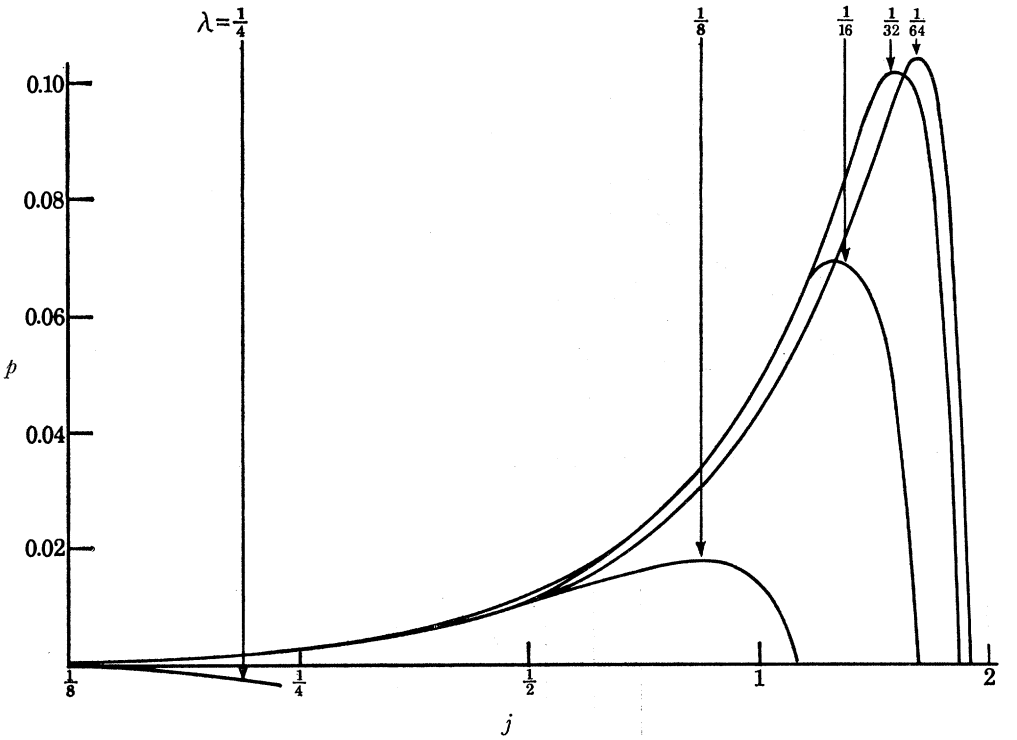

FIGURE 10. Numerical results giving the growth rate for the fourth motion, for the indicated resistivities λ.

growing fields have a phase velocity between 1.0 and 2.1. These phase velocities are in agreement with the heuristic arguments of § 7; the maximum amplitude of the x-component of both motions being 2.

For the second motion, from figure 8, the critical value of j decreases as the resistivity λ decreases below $\lambda = \frac{1}{8}$. For the third motion this critical value appears to tend to a constant $j = 0.42$. Also figure 9 indicates a separate branch of the growth rate curve around $j = 1$ for $\lambda \leqslant \frac{1}{16}$, which is quite surprising. Finally, for the fourth motion the critical value of j increases with decreasing λ, and is much larger than for the second and third motions. The maximum growth rate is also larger, and the near identity of the growth rates in $j < \frac{1}{2}$ for $\lambda \leqslant \frac{1}{8}$ is remarkable.

10. THE NUMERICAL METHODS

(a) *The truncated eigenvalue problem and convergence*

In the numerical solution of partial differential equations it is necessary to represent the unknown function using a finite number of variables. This can be done by making the variables the function values at a number of 'grid points', not necessarily uniformly spaced, with finite

differences used to approximate the derivatives. Alternatively, the variables can be a finite number of the coefficients in the expansion of the function in terms of an infinite set of known functions, with the approximation of setting the remainder to zero.

For an eigenvalue problem like equation (2.14), the set of eigenvalues found numerically will clearly depend on the number of variables used to represent the function. If there is no clear evidence of convergence as this number increases, no confidence can be placed in the results. The number of variables required for the accurate representation of a function will normally be greater if the function varies on a very small length scale in part of the relevant region, for example if it is of boundary-layer type.

Numerical study of the kinematic dynamo problem has been handicapped by the fact, proved by Cowling (1933), that a growing magnetic field cannot be axisymmetric or a function of only two Cartesian coordinates. Its accurate representation therefore requires a very large number of variables. Bullard & Gellman (1954) proposed a spherical dynamo model, with a steady non-axisymmetric motion, and expressed the condition for the maintenance of a steady field as an eigenvalue equation, with the magnetic Reynolds number as eigenvalue. To represent functions of the variables r, θ and ϕ, they used a finite sum of spherical harmonics for the θ and ϕ variation and represented the radial variation by finite difference methods. The need to store the resulting matrices in a computer imposed severe restrictions on the number of spherical harmonics and radial grid points which could be included. Their results seemed slightly encouraging with regard to convergence, but Lilley (1970) and Gibson & Roberts (1969, using a finite sum of Chebyshev polynomials for the radial variation), showed that the convergence was only apparent, and that even at their much better levels of approximation convergence could not be demonstrated.

It has been shown in this paper how motions which are functions of only two Cartesian coordinates can maintain and amplify fields of the form (2.8) which are functions of all three. In the corresponding eigenvalue equation (2.14), the eigenfunction $\boldsymbol{H}$ is a function of only two Cartesian variables, and can therefore be represented much more accurately than a function of three variables on a computer. The function $\boldsymbol{H}(y, z)$ could have been represented by its values on a uniformly spaced grid in the y–z plane, using finite differences for the differential operator $\mathscr{P}$ in equation (2.14). This method is used in a study (Roberts 1972*a*) of the dynamo action of axisymmetric motions $\boldsymbol{u}(r, \theta)$ in a sphere, with field solutions of the form

$$\boldsymbol{B} = \boldsymbol{H}(r, \theta) \exp(pt + \mathrm{i}m\phi),$$

cf. equation (2.8). It has the advantage that the matrix representing the differential operator $\mathscr{P}$ is sparse. But the eigenvalue problem was in fact solved by representing $\boldsymbol{H}(y, z)$ by a finite number of terms of the infinite Fourier sum (8.9), and using the Fourier analysed forms of the equations. With the particular motions (5.1), (6.1), (6.2) and (6.3) considered, the matrix representing $\mathscr{P}$ is still sparse. Further, the truncated Fourier series representation probably gives greater accuracy in the eigenvalue, with a given fixed number of variables to represent the function $\boldsymbol{H}(y, z)$, than the use of finite differences.

The exact Fourier-analysed equations (8.10) to (8.13) were therefore approximated by taking

$$\boldsymbol{h}^{(s)}_{m,n} = 0 \quad \text{for} \quad \max\{|m|, |n|\} > s, \tag{10.1}$$

for the first three motions, with $\boldsymbol{h}_{m,n}$ complex, and

$$\boldsymbol{h}^{(s)}_{m,n} = 0 \quad \text{for} \quad |m| + |n| > 2s, \tag{10.2}$$

for the fourth motion, with $\boldsymbol{h}_{m,n}$ real, and then ignoring the corresponding equations. The symmetry conditions given in table 2 on page 428 were used to reduce the number of independent components for each value of s. The eigenvalue p_s^* with the largest real part was then found, as described in § 10 (b) below, and its convergence with increasing s was studied.

Since all generalized eigenvectors of $\mathscr{P}$ satisfy homogeneous linear elliptic differential equations with infinitely differentiable coefficients and periodic boundary conditions, they are themselves infinitely differentiable, and therefore

$$|\boldsymbol{h}_{m,n}| = o(m^2+n^2)^{-k}, \tag{10.3}$$

as $m^2+n^2 \to \infty$, for all k. This fact was proved in the earlier paper (Roberts 1969) direct from the Fourier analysed equations. It indicates that the eigenvalues found numerically can be expected to converge as $s \to \infty$.

Let the eigensolutions $\boldsymbol{h}_{m,n}$ and $\boldsymbol{h}^{(s)}_{m,n}$ be normalized so that

$$g_{0,0} = 1, \tag{10.4}$$

and define z_r and $z_r^{(s)}$ by the equation

$$z_r = \max_{S_r} \{|f_{m,n}|, |g_{m,n}|\}, \tag{10.5}$$

the maximum being over the set S_r of values of m and n with $|m|+|n| = 2r$ for the fourth motion and with $\max\{|m|, |n|\} = r$ for the others (cf. equations (10.1) and (10.2)). For any eigensolution, including that with the eigenvalue having the largest real part, z_r tends to zero as r increases. This follows from equation (10.3). Further, for the approximate eigenvalue p_s^* with the largest real part, it is to be expected that $z_r^{(s)}$ will tend to decrease as r increases up to s, since eigensolutions with $\boldsymbol{h}^{(s)}_{m,n}$ large for large values of m and n will decay more rapidly. Thus it is to be expected that p_s^* will be a good approximation to p^* if z_s and $z_s^{(s)}$ are small. More precisely, the result,

$$|p_s^* - p^*| = O(z_s^{(s)})^2, \tag{10.6}$$

can be expected as s increases. Approximately, $z_s^{(s)}$ represents the order of magnitude of the effect of the unit $g_{0,0}$ in generating field components at the edge of the square defined by equations (10.1) and (10.2). The neglected components, of order $z_s^{(s)}$, therefore probably have an effect on $g_{0,0}$ of order $(z_s^{(s)})^2$. Equation (10.6) is amply confirmed by the numerical results presented in tables 4 to 6 below.

The magnetic field is increasingly of boundary-layer type as the resistivity λ decreases, with the field varying substantially on a length scale of asymptotic order $\lambda^{\frac{1}{2}}$ (Roberts 1972 b). Thus z_s and $z_s^{(s)}$ decrease to zero more slowly, and increasingly large values of s are therefore required for the eigenvalues p_s^* to converge.

Typical results for the convergence of the eigenvalues p_s^* with increasing s are given in table 4, for a variety of λ and j values for each motion. The corresponding values of $z_s^{(s)}$ are also shown, and confirm equation (10.6). Because of this result, most values of λ and j were studied for one value of s only; if $z_s^{(s)}$ was less than $\frac{1}{10}$ the result was regarded as satisfactory.

It was found that the value of s required for an accuracy of 3 significant figures in the dominant eigenvalue was practically independent of j for fixed λ; only when j took values substantially greater than one did it start to increase. The values of s which were used for each motion and each resistivity are shown in table 5, with corresponding order of magnitude for $z_r^{(s)}$. Where field solutions had a large growth rate, $z_r^{(s)}$ decreased more rapidly; this is to be expected, since the denominators in the series (11.13) for ϕ_{qr} are much larger.

TABLE 4. CONVERGENCE OF THE EIGENVALUES p_s

motion	λ	j	s	Re p_s	Im p_s	$z_s^{(s)}$
I	1	$\frac{1}{2}$	3	0.0840389		10^{-3}
			7	0.0840389		10^{-9}
			13	0.0840389		10^{-20}
	$\frac{1}{8}$	$\frac{1}{2}$	3	0.166		0.055
			5	0.169165		0.007
			7	0.1691710		0.0006
	$\frac{1}{32}$	1	8	0.1457		0.025
			9	0.14613		0.013
	$\frac{1}{64}$	1	11	0.1324		0.027
			13	0.13297		0.011
II	$\frac{1}{8}$	$\frac{1}{4}$	3	0.023347	$\pm$ 0.4676	0.19
			5	0.023345	$\pm$ 0.463825	0.023
	$\frac{1}{16}$	$\frac{1}{4}$	3	0.022	$\pm$ 0.53	0.38
			7	0.01593	$\pm$ 0.4768	0.02
III	$\frac{1}{2}$	$\frac{1}{2}$	4	$-$ 0.09832552	$-$ 0.426276455	10^{-3}
			5	$-$ 0.0983255641	$-$ 0.426276464	10^{-4}
			7	$-$ 0.0983255646	$-$ 0.426276464	10^{-7}
	$\frac{1}{32}$	0.294	6	0.0638	$-$ 0.5517	0.069
			8	0.06415	$-$ 0.5521	0.024
	$\frac{1}{32}$	1	8	0.0497	$-$ 1.934	0.09
	$\frac{1}{64}$	1	8	0.045	$-$ 1.98	0.32
	$\frac{1}{128}$	$\frac{1}{4}$	8	0.00550	$-$ 0.5002	0.27
			10	0.00627	$-$ 0.5006	0.20
			15	0.00671	$-$ 0.5015	0.066
	$\frac{1}{128}$	$\frac{1}{32}$	8	0.0000651	$-$ 0.06251	0.35
			10	0.0000604	$-$ 0.06254	0.26
			15	0.0000607	$-$ 0.06257	0.083
IV	$\frac{1}{4}$	1	6	$-$ 0.1556805		0.0043
			7	$-$ 0.15567850		0.0009
			8	$-$ 0.155678597		0.0002
	$\frac{1}{64}$	$\frac{1}{16}$	14	0.000189		0.17
			15	0.000206		0.10
			20	0.0001984		0.025
			25	0.0001987		?
	$\frac{1}{256}$	$\frac{1}{16}$	20	0.000065		0.47
			30	0.000100		0.14

TABLE 5. THE VALUES OF s USED FOR EACH RESISTIVITY, AND THE CORRESPONDING $z_s^{(s)}$ MAGNITUDES

motion	λ =	2	1	$\frac{1}{2}$	$\frac{1}{4}$	$\frac{1}{8}$	$\frac{1}{64}$	$\frac{1}{32}$	$\frac{1}{16}$	$\frac{1}{128}$	$\frac{1}{256}$
I	s =	2	2	3	4	5	8	9	13	—	—
	$z_s^{(s)}$ =	0.003	0.016	0.007	0.007	0.008	0.003	0.02	0.01	—	—
II	s =	2	3	3	4	5	7	8	—	—	—
	$z_s^{(s)}$ =	0.006	0.002	0.015	0.015	0.015	0.02	0.08	—	—	—
III	s =	—	5	5	5	6	8	8	8	15	—
	$z_s^{(s)}$ =	—	10^{-6}	10^{-4}	0.002	0.008	0.003	0.03	0.15	0.07	—
IV	s =	—	5	5	6	8	10	14	14	—	30
	$z_s^{(s)}$ =	—	10^{-4}	0.001	0.004	0.007	0.02	0.02	0.15	—	0.14

PHILOSOPHICAL TRANSACTIONS OF THE ROYAL SOCIETY A MATHEMATICAL, PHYSICAL & ENGINEERING SCIENCES

Finally, no attempt is made here to describe the growing fields in detail, or to evaluate and display the sums of the finite Fourier series. But to give some slight idea of the extent of the development of thin layers, and of the pattern of convergence, results for $z_r^{(s)}$, for a variety of cases, are given in table 6.

TABLE 6. ORDERS OF MAGNITUDE $z_r^{(s)}$ OF THE FOURIER COMPONENTS OF THE MAGNETIC FIELDS

	λ	j	s	0	1	2	3	4	5	6	7	8	9	10	11	12	13	14
	1	$\frac{1}{2}$	8	1	0.17	0.021	0.001	10^{-4}	10^{-6}	10^{-7}	10^{-9}	10^{-11}	—	—	—	—	—	—
	$\frac{1}{8}$	$\frac{1}{2}$	7	1	0.29	0.12	0.05	0.02	0.007	0.002	0.001	—	—	—	—	—	—	—
	$\frac{1}{64}$	1	13	1	0.45	0.32	0.21	0.14	0.11	0.08	0.06	0.04	0.03	0.02	0.015	0.01	0.01	—
I	50	$\frac{1}{100}$	3	1	10^{-2}	10^{-6}	10^{-9}	—	—	—	—	—	—	—	—	—	—	—
	$\frac{1}{8}$	$\frac{1}{4}$	5	1	0.70	0.34	0.16	0.068	0.023	—	—	—	—	—	—	—	—	—
	$\frac{1}{32}$	$\frac{1}{4}$	8	1	0.84	0.55	0.37	0.27	0.19	0.12	0.08	0.07	—	—	—	—	—	—
II	$\frac{1}{2}$	0.179	4	1	0.45	0.067	0.007	0.001	—	—	—	—	—	—	—	—	—	—
	$\frac{1}{8}$	$\frac{1}{4}$	6	1	0.36	0.14	0.073	0.028	0.009	0.002	—	—	—	—	—	—	—	—
	$\frac{1}{32}$	$\frac{1}{4}$	8	1	0.42	0.23	0.14	0.10	0.070	0.045	0.030	0.025	—	—	—	—	—	—
	$\frac{1}{64}$	$\frac{1}{8}$	8	1	0.50	0.47	0.42	0.34	0.27	0.22	0.18	0.18	—	—	—	—	—	—
V	$\frac{1}{4}$	$\frac{1}{400}$	14	1	0.53	0.46	0.14	0.063	0.016	0.005	0.001	10^{-4}	10^{-4}	10^{-5}	10^{-6}	10^{-7}	10^{-8}	10^{-9}
	$\frac{1}{64}$	$\frac{1}{6400}$	14	1	0.23	0.98	0.35	0.89	0.35	0.69	0.30	0.48	0.22	0.32	0.14	0.22	0.07	0.16
	$\frac{1}{1000}$	10^{-6}	14	1	0.027	1.00	0.046	0.999	0.058	0.997	0.062	0.994	0.058	0.989	0.046	0.983	0.027	0.979

(*b*) *The eigenvalue method*

The method of inverse iteration (see, for example, Wilkinson 1965, pp. 619, 628) was used to find the eigenvalue with the largest real part, for each matrix derived above. The finite-dimensional eigenvalue problem can be written as

$$P\boldsymbol{x} = p\boldsymbol{x}, \tag{10.7}$$

where P is an $N \times N$ matrix, complex-valued except for the fourth motion, and $\boldsymbol{x}$ is the vector of $f_{m,n}$ and $g_{m,n}$ components, ordered as described below. With an initial approximation,

$$\{p_0, \boldsymbol{x}_0\}, \tag{10.8}$$

to the eigensolution, the vectors,

$$\boldsymbol{x}_n = \epsilon_n (P - p_0 I)^{-1} \boldsymbol{x}_{n-1} \tag{10.9}$$

$$= \epsilon_1 \epsilon_2 \ldots \epsilon_n (P - p_0 I)^{-n} \boldsymbol{x}_0, \tag{10.10}$$

are evaluated, with ϵ_n defined so that $g_{0,0} = 1$, (10.11)

say, at each stage. The iteration is stopped if for any value of n,

$$|\boldsymbol{x}_n - \boldsymbol{x}_{n-1}| < \delta, \tag{10.12}$$

where $|\boldsymbol{x}|$ denotes the sum of the moduli of the components and δ is a small test parameter which was usually chosen as 10^{-10} since the computer worked to about 12 significant figures. Using equations (10.9) and (10.12), with $\delta = 0$ and $\boldsymbol{x}_n = \boldsymbol{x}$,

$$P\boldsymbol{x} = (p_0 + \epsilon_n)\boldsymbol{x}, \tag{10.13}$$

and the eigensolution has been found. Otherwise the iteration (10.9) is stopped at a certain value of n, which was usually 20, and

$$\{p_0 + \epsilon_n, \boldsymbol{x}_n\} \tag{10.14}$$

is used as the new approximation (10.8) to the eigensolution. The process above is then repeated until convergence is obtained.

In the analysis of the method, it will be assumed that the matrix P in equation (10.7) has N complex eigensolutions,

$$\{p^{(j)}, \boldsymbol{x}^{(j)}\} \quad (j = 1, 2, \ldots, N),$$

with the eigenvectors $\boldsymbol{x}^{(j)}$, chosen to satisfy equation (10.11), independent and complete. This is not so in general unless generalized eigensolutions are included (cf. § I, appendix B); the extension of the analysis below to the general case is straightforward. Then, with

$$\boldsymbol{x}_n = \Sigma a_n^{(j)} \boldsymbol{x}^{(j)}, \tag{10.15}$$

equation (10.10) implies that

$$a_n^{(j)} = \epsilon_1 \epsilon_2 \ldots \epsilon_n (p^{(j)} - p_0)^{-n} a_0^{(j)}, \tag{10.16}$$

and the factors ϵ_n are determined by the conditions,

$$\sum_{j=1}^{N} a_n^{(j)} = 1, \tag{10.17}$$

from equation (10.11). So

$$a_n^{(j)} \to 0, \quad \text{as} \quad n \to \infty, \tag{10.18}$$

unless $p^{(j)}$ is one of the eigenvalues closest to p_0 in the complex plane. If $p^{(1)}$ is the closest,

$$a_n^{(1)} \to 1 \quad \text{as} \quad n \to \infty, \tag{10.19}$$

as required. Even if 20 iterations do not give convergence, the new initial approximation (10.14) will probably be very good. It is clear that the first eigenvector approximation $\boldsymbol{x}_0$ need not be an approximation at all; in fact $\boldsymbol{x}_0$ was frequently zero except for the $g_{0,0}$ component which was unity.

In order to evaluate $(P - p_0 I)^{-1} \boldsymbol{x}_{n-1}$ in equation (10.9), the matrix $P - p_0 I$ is expressed, using Gaussian elimination without interchange, as

$$P - p_0 I = LU, \tag{10.20}$$

where L is lower triangular with unit diagonal, and U is upper triangular. The components are ordered in such a way that P has the banded structure,

$$P_{ij} = 0 \quad \text{for} \quad |i - j| > B,$$

with minimum band-width $2B + 1$. Only this band of $P - p_0 I$ is stored in the computer, and in the triangular decomposition the components are replaced by the corresponding components of U and the corresponding non-diagonal components of L. The triangular decomposition is done just once, and requires a number of arithmetical operations of order NB^2. For each step of the iteration, the solution of equation (10.9), in the form,

$$\boldsymbol{x}_n = \epsilon_n U^{-1} L^{-1} \boldsymbol{x}_{n-1}, \tag{10.21}$$

requires a number of operations of order $2NB$. Thus for $B = 40$, the triangular decomposition takes a time comparable with that for 20 iterations.

The initial approximations p_0 to the eigenvalues were chosen as follows. If the same problem had just been studied with a smaller s, the result was used. Otherwise if, as was usually the case, a succession of values of j were being studied for fixed values of λ and s, the result with the previous value of j was generally used. Sometimes the real part of these previous values was slightly increased, but this precaution was found to be unnecessary. The above scheme usually gave very

rapid convergence, with n typically between 3 and 7. The initial values for each λ value had a large positive real part, to be sure of finding the eigenvalue with the largest real part. It was easy to find other eigenvalues, and to follow their variation with j for fixed λ; it was by this means that the separate branch near $j = 1$ for the third motion, shown for $\lambda = \frac{1}{16}$ in figure 9, was found. For $\lambda = \frac{1}{32}$ and $\frac{1}{64}$ only the values of the growth rate at $j = 1$ are shown; for $\lambda = \frac{1}{64}$ the result for $\mathrm{Re}\, p$ is probably only accurate to within 0.01 or so. An extensive search did not reveal any such branch for the other motions; the results presented almost certainly give the eigenvalues with the largest real part.

No particular difficulty was experienced over eigenvalues roughly equidistant in the complex plane from the initial approximation p_0. The iteration described always converged to some eigenvalue eventually, after going through a sequence of new initial approximate eigensolutions of the form (10.14). For the fourth motion real eigensolutions were assumed, although with equation (8.13) complex eigensolutions in conjugate pairs are also possible. For certain cases, with negative initial approximations p_0, the eigenvalues closest in the complex plane were apparently such complex pairs; in such cases there was no sign of convergence according to equation (10.12) until the new initial approximations to the eigenvalue, determined according to the form (10.14), had their closest eigenvalue real.

The inverse iteration eigenvalue method as described is readily adaptable to matrices so large that the band cannot all be held simultaneously in main storage, and additional storage devices have to be used. The process (10.20) of triangular decomposition only uses $B+1$ rows of the matrix at a time, and the process (10.21) only uses one row of L at a time and then one row of U at a time. Thus with the band of P_{ij} components satisfying

$$|i-j| \leqslant B$$

stored by rows, only a relatively small number of rows need be in main storage at a time. The Cambridge University Titan computer, used during 1967, gave 35 000 words of storage, with 12 significant figures held, and a 5 μs operation time. There was no system to give the programmer virtual storage implicitly, and programs had to be written to transfer numbers to and from magnetic tape during the processes of setting up the matrix, of triangular decomposition, and of the n applications of equation (10.21). This was done for the third and fourth motions only, and typical results are described in table 4 on page 435. The largest matrices studied were real matrices of order 1861, with band-width 129, for which eigenvalues were found in eight minutes, excluding the time for tape transfers on a time-shared machine, and complex matrices of order 481 with band-width 68, for which eigenvalues were found in five minutes computation time. The disadvantage was that the execution times, with tape transfers included, were five times as long, and the additional information to be gained by taking the resistivities down another factor of 2 was not felt to be worth the computing time which would have been involved.

Finally, the accuracy of the eigenvalue method was always checked by evaluating the terms in each component of $P\boldsymbol{x} - p\boldsymbol{x}$, and dividing their sum by the sum of their moduli. The result was always 10^{-10} or smaller. Further, the eigenvalues obtained from widely differing initial approximations (10.8) agreed to 10 significant figures. Thus no difficulties were experienced with the method due to not using any interchange in the Gaussian elimination for the triangular decomposition (10.20), in spite of Wilkinson's warnings (1965, p. 629).

11. The tensor ϕ_{qr}

It is shown in § 6 that the three additional illustrative motions (6.1) to (6.3) are not first-order dynamos for any resistivity λ. The determinants of the symmetric parts of the trailing minors of the tensors α_{qr}, shown in table 2, on page 428 are respectively negative, zero and zero, and thus from § 3 there is no dynamo action to first order in the components of $\boldsymbol{j}$. The numerical work shows that all three motions act as dynamos to higher order in the components of $\boldsymbol{j}$, for sufficiently small resistivities, but it has not been found possible to prove this analytically. The multiple-scale versions (6.4) to (6.6) of the three motions have therefore been introduced, and their dynamo action to second order in $\boldsymbol{j}$ is established in §§ 12 and 13. The analytic methods required are developed in this section.

In order to demonstrate that a first-order analysis for small $\boldsymbol{j}$ is reasonable, it was shown in the first paper, in § I, appendix D, how the eigensolutions $\{p, \boldsymbol{H}(x)\}$ can in principle be found to second and higher orders in $\boldsymbol{j}$. But the method is of little practical value, and is not used here.

Attention is confined to vectors $\boldsymbol{j}$ in the x-direction, so that $\boldsymbol{j} = j\hat{\boldsymbol{x}}$, and the eigenvalue equation is used in the Fourier analysed forms (8.10), (8.11) and (8.12) for the three motions. These equations are written as

$$\{p^* + m^2(\lambda k^2) + n^2(\lambda l^2)\}\boldsymbol{h}_{m,n} = \{\mathscr{U}\boldsymbol{h}\}_{m,n}. \tag{11.1}$$

The set of Fourier components $\boldsymbol{h}_{m,n}$ is now partitioned into the zero component $\boldsymbol{h}_{0,0}$, denoted by $\boldsymbol{h}^{\mathrm{A}}$, and the remaining components, denoted by $\boldsymbol{h}'$. The notation is natural since $\boldsymbol{h}^{\mathrm{A}}$ and $\boldsymbol{h}'$ represent respectively the average and oscillatory parts $\boldsymbol{H}^{\mathrm{A}}$ and $\boldsymbol{H}'(\boldsymbol{x})$ of $\boldsymbol{H}(\boldsymbol{x})$, according to equations (2.2) and (2.4), (8.6) and (8.9). In fact

$$\boldsymbol{h}_{0,0} = (f_{0,0}, g_{0,0}) = (kH_y^{\mathrm{A}}, lH_z^{\mathrm{A}}). \tag{11.2}$$

With this partitioning of $\boldsymbol{h}_{m,n}$, equation (11.1) can be partitioned as

$$p^*\boldsymbol{h}^{\mathrm{A}} = \mathscr{U}^{\mathrm{A}\prime}\boldsymbol{h}', \tag{11.3}$$

$$\{p^* + m^2(\lambda k^2) + n^2(\lambda l^2)\}\boldsymbol{h}' = \mathscr{U}''\boldsymbol{h}' + \mathscr{U}'^{\mathrm{A}}\boldsymbol{h}^{\mathrm{A}}. \tag{11.4}$$

Suppose now that equation (11.4) is soluble for $\boldsymbol{h}'$, the set of $\boldsymbol{h}_{m,n}$ components with m and n not both zero, as a function of λ, j and p^* and as a linear function of $\boldsymbol{h}^{\mathrm{A}} = \boldsymbol{h}_{0,0}$. Then substitution in equation (11.3) gives the equation

$$p^*(\boldsymbol{h}^{\mathrm{A}})_q = \phi_{qr}(\boldsymbol{h}^{\mathrm{A}})_r, \tag{11.5}$$

where ϕ_{qr} is a complex 2×2 matrix, a function of λ, j and p^*. This eigenvalue problem is analogous to that defined by equations (3.1) and (3.2); in fact

$$\phi_{qr} = \mathrm{i}j\begin{bmatrix} -\alpha_{32} & -(k/l)\alpha_{33} \\ (l/k)\alpha_{22} & \alpha_{23} \end{bmatrix} + O(j^2). \tag{11.6}$$

The k/l and l/k factors appear because of the relation (11.2) between $\boldsymbol{h}^{\mathrm{A}}$ and $\boldsymbol{H}^{\mathrm{A}}$.

The tensor ϕ_{qr} in the eigenvalue equation (11.5) is itself a nonlinear function of the eigenvalue p^*. The equation is nevertheless applicable in two senses. First, deductions concerning the shape of ϕ_{qr} for the three motions are made in § 12, and extended to general values of λ, j and p^* in appendix B. These results are used to show that for the third and fourth motions every eigenvalue is degenerate, with an even number of eigensolutions. Corresponding deductions for the second motion simplify the analysis in § 13. Secondly, the detailed application of equation (11.5) is practicable if for

$$|p^*| < c, \tag{11.7}$$

where c is a constant, ϕ_{qr} has two differentiable eigenvalues $\phi(p^*)$, satisfying

$$|\phi| \ll c, \quad |\mathrm{d}\phi/\mathrm{d}p^*| \ll 1. \tag{11.8}$$

In this case, the iteration defined by

$$p_0^* = 0, \quad p_{n+1}^* = \phi(p_n^*), \tag{11.9}$$

converges very rapidly to the two eigenvalues p^* with modulus less than c, and p_1^* is a very good approximation. This iteration is used to demonstrate dynamo action in §13. For the second and third motions, p_1^* is dominated by its imaginary part, and it is necessary to consider p_2^* to get an asymptotically valid approximation to the real part.

It remains to find a method for the solution of equation (11.4), and the determination of the 2×2 tensor ϕ_{qr}. Suppose that the series

$$\boldsymbol{h}' = \sum_{\omega=0}^{\infty} \boldsymbol{h}'_\omega \tag{11.10}$$

is uniformly convergent, with $\boldsymbol{h}'_\omega$ defined by the relations

$$\left.\begin{aligned} \boldsymbol{h}'_0 &= \{p^* + m^2(\lambda k^2) + n^2(\lambda l^2)\}^{-1} \mathscr{U}'^{\mathrm{A}} \boldsymbol{h}^{\mathrm{A}}, \\ \boldsymbol{h}'_{\omega+1} &= \{p^* + m^2(\lambda k^2) + n^2(\lambda l^2)\}^{-1} \mathscr{U}'' \boldsymbol{h}'_\omega. \end{aligned}\right\} \tag{11.11}$$

Then $\boldsymbol{h}'$ is the unique solution of equation (11.4), and equation (11.3) can be written as

$$p^* \boldsymbol{h}^{\mathrm{A}} = \sum_{\omega=0}^{\infty} \mathscr{U}^{\mathrm{A}\prime} [\{p^* + m^2(\lambda k^2) + n^2(\lambda l^2)\}^{-1} \mathscr{U}'']^{\omega} \{p^* + m^2(\lambda k^2) + n^2(\lambda l^2)\}^{-1} \mathscr{U}'^{\mathrm{A}} \boldsymbol{h}^{\mathrm{A}}. \tag{11.12}$$

The operators $u^{\mathrm{A}\prime}$, u'' and u'^{A} are determined by the right-hand sides of equations (11.3), (11.4) and (11.1) in the forms (8.10) to (8.12). Thus

$$\phi_{qr} = \sum_{\omega=2}^{\infty} \sum_{(\omega)} \frac{\prod_{i=1}^{\omega} s_i}{\prod_{i=1}^{\omega-1} \{p^* + m_i^2(\lambda k^2) + n_i^2(\lambda l^2)\}}, \tag{11.13}$$

where $\sum_{(\omega)}$ denotes a sum over all 'closed sequences' of ω 'interaction steps', from a vector component $f_{0,0}$ or $g_{0,0}$ (according as r is 1 or 2), through a sequence of components

$$f_{m_i, n_i} \quad \text{or} \quad g_{m_i, n_i} \quad (i = 1, 2, \ldots, \omega - 1),$$

to a component $f_{0,0}$ or $g_{0,0}$ (according as q is 1 or 2). The integers m_i and n_i cannot both be zero for any i. Each interaction step is an x-, y- or z-convection, or a distortion of a g-component into an f-component or vice versa, as allowed by equations (8.10), (8.11) or (8.12), and s_i is the corresponding multiplying factor. Thus for the second motion, according to equation (8.10) with $m = 3$ and $n = 4$, s_i is $\frac{1}{2}(Vk)$ for the distortion $g_{3,3} \to f_{3,4}$ and is $-2(Wl)$ for the z-convection $f_{2,4} \overset{W}{\to} f_{3,4}$. The symbols $\overset{U}{\to}$, $\overset{V}{\to}$ and $\overset{W}{\to}$ are used to indicate whether a convective interaction step is an x-, y- or z-convection in the obvious way. A typical closed sequence of interaction steps, for the second motion, is $f_{0,0} \to g_{1,0} \to g_{0,0}$; the corresponding contribution to ϕ_{21} is

$$(\tfrac{1}{2}Wl)\,(-\tfrac{1}{2}\mathrm{i}Uj),$$

from equation (8.10).

Sufficient conditions for the rapid convergence of the series (11.10) (11.12) and (11.13), for the three motions, are derived in §13. Equation (11.13) is also used in §12, in deriving results

about the shape of the tensor ϕ_{qr}. It is shown in appendix B that these results apply even when the series (11.10) is not convergent.

12. The shape of ϕ_{qr} for the three multiple-scale motions

For the three multiple-scale motions (6.4), (6.5) and (6.6), the 2×2 tensor ϕ_{qr}, defined in § 11 as a function of λ, j and p^*, takes the respective forms,

$$\begin{bmatrix} \kappa & \mu \\ \nu & \kappa \end{bmatrix}, \tag{12.1}$$

$$\begin{bmatrix} \kappa & 0 \\ 0 & \kappa \end{bmatrix}, \tag{12.2}$$

and

$$\begin{bmatrix} \kappa & 0 \\ 0 & \kappa \end{bmatrix}, \tag{12.3}$$

where the functions κ are of course different for the different motions. These results are established below for cases where the series (11.13) for ϕ_{qr} is convergent; they are extended to the general case in appendix B.

To prove the equality of the diagonal terms, consider the one-to-one correspondence in equation (11.13) between closed sequences of interaction steps contributing to ϕ_{11} and closed sequences contributing to ϕ_{22}, defined by taking the sequence of (m_i, n_i) values in reverse and replacing all f-components by g-components and vice versa. Thus in an (m, n) diagram a convection step in one direction becomes a convection step in the other direction, and a distortion step from an f-component to a g-component in one direction becomes a distortion step from an f-component to a g-component in the opposite direction in the (m, n) diagram. From equations (8.10) to (8.12) the multiplying factor s_i is unaltered except for a change of sign with y- and z-convections and with fourth motion x-convections. It is now established, separately for the three motions, that the corresponding contributions to ϕ_{11} and ϕ_{22} are equal. Clearly the denominator products in equation (11.13) are identical, it is therefore only necessary to prove that the signs of the products $\prod_1^{\omega} s_i$ are the same. For the second and third motions, this requires that the total number of y- and z-convection interaction steps is even; for the fourth it requires that the total number of convection steps is even.

For the second motion, consider closed sequences of interaction steps, with an odd total of y- and z-convections, contributing to a particular term of ϕ_{qr} in equation (11.13). Further, consider the one-to-one corresponedence between them defined by just changing the sign of n_i in all the f_{m_i, n_i} and g_{m_i, n_i} components. This is one-to-one since the n_i cannot all be zero. The corresponding denominators in equation (11.13) are identical; so are the numerators except for a sign change for y- and z-convections. So the total contribution is zero, and closed interaction step sequences with an odd number of y- and z-convections are negligible. The tensor shape (12.1) follows. Further, contributions to κ are even in iUj, and contributions to μ and ν are odd, since the total number of interaction steps is even.

For the third motion, x-convections change $m+n$ by an even number, while distortion interaction steps and y- and z-convections change it by unity. The number of distortions in closed interaction sequences contributing to ϕ_{11} or ϕ_{22} is even. Thus so is the total number of y- and z-convections, and ϕ_{11} and ϕ_{22} are equal.

For the fourth motion, x-convection interaction steps change m by unity and leave $m-n$ unchanged, while distortions and y- and z-convections change m by an even number and change $m-n$ by two. Therefore there are an even number of x-convections, an even number of distortions, and an even number of y- and z-convection interaction steps, in any closed interaction step sequence contributing to ϕ_{11} or ϕ_{22}. Thus the diagonal terms are again equal.

To prove that the off-diagonal terms of ϕ_{qr} are zero for the third and fourth motions, the closed interaction sequences contributing to ϕ_{12} in equation (11.13) are divided into pairs under the same one-to-one correspondence, with the sequence of (m_i, n_i) values taken in reverse and with f-components replaced by g-components and vice versa. The denominator products in equation (11.13) are identical, so it is only necessary to prove that the s_i products change sign. For the third motion this requires that the number of y- and z-convections is identically odd, while for the fourth motion the total number of convection interaction steps must be proved odd. These two facts follow immediately from the arguments of the last two paragraphs, since the number of distortions is odd. Thus ϕ_{12} is zero. Similarly, ϕ_{21} is zero, and the shapes (12.2) and (12.3) have been established for the third and fourth motions.

TABLE 7. INTERACTION STEP SEQUENCE CONTRIBUTION TO ϕ_{qr}

motion	II		III	IV
term of ϕ_{qr} ...	$\phi_{11} = \phi_{22} = \kappa$	$\phi_{12} = \mu$ $\phi_{21} = \nu$	$\phi_{11} = \phi_{22} = \kappa$	$\phi_{11} = \phi_{22} = \kappa$
numbers of interaction steps in equation (11.13)				
x-convections	even	odd	positive	even
y- and z-convections	even	even	even	even
distortions	even	odd	even	even

The shapes of the trailing minors of the tensor α_{qr} for the three multiple-scale motions can be now deduced from equations (11.6), and are

$$\begin{bmatrix} a & 0 \\ 0 & d \end{bmatrix}, \tag{12.4}$$

$$\begin{bmatrix} 0 & b \\ -b & 0 \end{bmatrix}, \tag{12.5}$$

and

$$\begin{bmatrix} 0 & 0 \\ 0 & 0 \end{bmatrix}, \tag{12.6}$$

respectively. The off-diagonal terms are zero for the second and fourth motions since closed interaction step sequences include an even number of x-convections and thus give an even number of factors Uj in equation (11.13). Thus the diagonal terms of ϕ_{qr} are zero to first order in j.

The above results concerning the numbers of the different kinds of interaction steps in sequence contributing in equation (11.13) to the different terms of the 2×2 tensor ϕ_{qr} are summarized in table 7.

13. ANALYTIC RESULTS FOR THE ADDITIONAL ILLUSTRATIVE MOTIONS

Using the results of §§ 11 and 12, it is now proved that each of the multiple-scale forms (6.4), (6.5) and (6.6) of the three additional illustrative motions (6.1), (6.2) and (6.3) can give dynamo

action in a certain limit. The stages of the analysis are summarized in table 8 for the three motions. The first stage is to establish conditions on the relative magnitudes of the inverse time-scales λk^2, λl^2, Uj, Vk, Wl and p^* sufficiently strong for the series (11.10) for $\boldsymbol{h}'$ to converge very rapidly, but sufficiently weak that dynamo action is not excluded. With the assumptions,

$$\lambda k^2 \ll \lambda l^2, \tag{13.1}$$

$$|p^*| < \tfrac{1}{2}\lambda k^2 \tag{13.2}$$

(cf. equation (11.7)), the denominators $p^* + m^2(\lambda k^2) + n^2(\lambda l^2)$ in equations (11.11) to (11.13) are dominated by the term $n^2(\lambda l^2)$ unless n is zero. Thus the assumptions,

$$Uj/\lambda l^2 \ll 1, \tag{13.3}$$

$$Vk/\lambda l^2 \ll 1, \tag{13.4}$$

$$Wl/\lambda l^2 \ll 1, \tag{13.5}$$

ensure that for interaction steps in equation (11.11) ending at field components with n non-zero the resulting field component is much less than the original. The corresponding conditions, $Uj/\lambda k^2 \ll 1$, etc., are not imposed, so for interaction steps ending at field components with $n = 0$, the resulting field component may be much larger than its cause. Instead, the weaker condition is imposed that for any sequence of interaction steps starting and finishing with g-components with $n = 0$ or with f-components with $n = 0$, the product of all the factors involved is much less than one. It is only necessary to consider short sequences, since the product of the factors for longer sequences is always expressible as the product of short sequence factors and of factors of the form (13.3), (13.4) or (13.5). The conditions (13.1) to (13.5), together with these further conditions, will imply that for any natural norm,

$$\|[\{p^* + m^2(\lambda k^2) + n^2(\lambda l^2)\}^{-1}\mathscr{U}'']^{\omega}\|^{1/\omega} \ll 1 \tag{13.6}$$

for sufficiently large ω, thus ensuring the rapid convergence of equation (11.12).

Sequences of interaction steps going from a $g_{m_1,0}$ component to an $f_{m_2,0}$ component and not involving convection in the x-direction (i.e. only involving mutliples of Vk or Wl) are ignored in this analysis, since the sum of the contributions from all such sequences is identically zero. For example, the factors corresponding to the two sequences for the second motion

$$g_{4,0} \xrightarrow{V} g_{4,1} \to f_{4,0}, \quad g_{4,0} \to f_{4,1} \xrightarrow{V} f_{4,0},$$

(V denoting convection by the y-component), are, from equations (11.11) and (8.10),

$$\frac{-4(\frac{1}{2}Vk)}{\{p^* + 16(\lambda k^2) + (\lambda l^2)\}} \frac{\frac{1}{2}Vk}{\{p^* + 16(\lambda k^2)\}},$$

$$\frac{\frac{1}{2}Vk}{\{p^* + 16(\lambda k^2) + (\lambda l^2)\}} \frac{4(\frac{1}{2}Vk)}{\{p^* + 16(\lambda k^2)\}},$$

and their sum is identically zero. The reason for this identical cancellation follows. Set Uj to zero on the right-hand sides of any of the equations (8.10) to (8.12), and define $\mathscr{U}$ appropriately in equation (11.1). Then the condition,

$$(m, n) \cdot \boldsymbol{h}_{m,n} = 0, \tag{13.7}$$

for some particular m and n, implies that for any r and s,

$$(r, s) \cdot \{\mathscr{U}\boldsymbol{h}_{m,n}\}_{r,s} = 0. \tag{13.8}$$

TABLE 8. SUMMARY OF THE ANALYTIC RESULTS FOR THE MULTIPLE-SCALE MOTIONS

		II(8.10)	III(8.11)	IV(8.12)
tion and Fourier equation	...			
pes of the tensor ϕ_{qr} l of the trailing minor κ_{rs}		$\begin{bmatrix}\kappa & \mu\\ \nu & \kappa\end{bmatrix}\begin{bmatrix}a & 0\\ 0 & d\end{bmatrix}$	$\begin{bmatrix}\kappa & 0\\ 0 & \kappa\end{bmatrix}\begin{bmatrix}0 & b\\ -b & 0\end{bmatrix}$	$\begin{bmatrix}\kappa & 0\\ 0 & \kappa\end{bmatrix}\begin{bmatrix}0 & 0\\ 0 & 0\end{bmatrix}$
ıditions for convergence				
$\frac{Vk)^2}{^2)\ (\lambda l^2)} \ll 1$ from the		$\frac{(Uj)}{(\lambda k^2)} \ll 1$ from the	$\frac{(Uj)^2}{(\lambda k^2)\ (\lambda l^2)} \ll$ from	$\frac{(Uj)^2}{(\lambda k^2)\ (\lambda l^2)} \ll 1$ from
uence $f_{m,0} \to f_{m,1} \to f_{m,0}$,		sequence $f_{m,0} \xrightarrow{U} f_{m+1,0}$,	$f_{m,0} \xrightarrow{U} f_{m+1,1} \xrightarrow{U} f_{m,0}$,	$f_{m,0} \xrightarrow{U} f_{m+1,1} \xrightarrow{U} f_{m,0}$,
$\frac{l)}{^2)} \ll 1$ from $f_{m,n} \xrightarrow{W} f_{m+1,n}$,		$\frac{(Uj)\ (Vk)\ (Wl)}{(\lambda k^2)^2(\lambda l^2)} \ll 1$ from $g_{m,0} \xrightarrow{U} g_{m,1} \to f_{m,0} \to g_{m+1,0}$.	$\frac{(Uj)\ (Vk)\ (Wl)}{(\lambda k^2)^2(\lambda l^2)} \ll 1$ from $g_{m,0} \xrightarrow{U} g_{m+1,1} \to f_{m+1,0} \to g_{m,0}$.	$\frac{(Uj)^2(Vk)\ (Wl)}{(\lambda k^2)^2(\lambda l^2)^2} \ll 1$ from $g_{m,0} \xrightarrow{U} g_{m+1,1} \xrightarrow{U} g_{m+2,2} \to f_{m+2,0} \to g_{m+}$
ıtributions to ϕ_{qr}, with mber of sequences and ical sequence		$-\frac{1}{2}\frac{(Uj)^2}{(\lambda k)^2}$ to κ from 2 like $g_{0,0} \xrightarrow{U} g_{1,0} \xrightarrow{U} g_{0,0}$,	$-\frac{(Uj)^2}{(\lambda l^2)}$ to κ from 4 like $g_{0,0} \xrightarrow{U} g_{1,1} \xrightarrow{U} g_{0,0}$,	$-\frac{1}{2}\frac{(Uj)^2}{(\lambda l)^2}$ to κ from 2 like $g_{0,0} \xrightarrow{U} g_{1,1} \xrightarrow{U} g_{0,0}$,
		$-\frac{1}{2}\frac{(Uj)^2(Vk)\ (Wl)}{(\lambda k^2)^2(\lambda l^2)}$ to κ from 8 like $g_{0,0} \xrightarrow{U} g_{1,0} \xrightarrow{U} g_{1,1} \to f_{1,0} \to g_{0,0}$,	$-\mathrm{i}\frac{(Uj)\ (Vk)\ (Wl)}{(\lambda k^2)\ (\lambda l^2)}$ to κ from 8 like $g_{0,0} \to f_{0,1} \xrightarrow{U} f_{1,0} \to g_{0,0}$,	$\frac{3}{16}\frac{(Uj)^2(Vk)\ (Wl)}{(\lambda k^2)\ (\lambda l^2)^2}$ to κ from 6 like $g_{0,0} \xrightarrow{U} g_{1,1} \to f_{1,-1} \xrightarrow{U} f_{2,0} \to g_{0,0}$.
		$-\mathrm{i}\frac{(Uj)\ (Vk)}{(\lambda l^2)}$ to μ from 4 like $g_{0,0} \to f_{0,1} \xrightarrow{U} f_{0,0}$,	$-\frac{1}{8}\frac{(Uj)^2(Vk)^2(Wl^2)^2}{(\lambda k^2)^3(\lambda l^2)^2}$ to κ from 32 sequences like $g_{0,0} \xrightarrow{U} g_{1,1} \to f_{1,0} \to g_{2,0}$ $\xrightarrow{U} g_{1,1} \to f_{1,0} \to g_{0,0}$.	
		$-\mathrm{i}\frac{(Uj)\ (Wl)}{(\lambda k^2)}$ to ν from 4 like $f_{0,0} \to g_{1,0} \xrightarrow{U} g_{0,0}$,		
		$-\frac{\mathrm{i}}{2}\frac{(Uj)\ (Vk)\ (Wl)^2}{(\lambda k^2)^2(\lambda l^2)}$ to ν from 8 like $f_{0,0} \to g_{1,0} \xrightarrow{U} g_{1,1} \to f_{1,0} \to g_{0,0}$.		
dition for growth		$\frac{(Vk)^2(Wl)^2}{(\lambda k^2)^2(\lambda l^2)^2} \gg 1$	$\frac{(Vk)^2(Wl)^2}{(\lambda k^2)^3(\lambda l^2)} \gg 1$	$\frac{(Vk)\ (Wl)}{(\lambda k^2)\ (\lambda l^2)} \gg 1$
minant term in Re p		$\frac{1}{2}\frac{(Uj)^2(Vk)^2(Wl)^2}{(\lambda k^2)^3(\lambda l^2)^2}$	$\frac{7}{8}\frac{(Uj)^2(Vk)^2(Wl)^2}{(\lambda k^2)^3(\lambda l^2)^2}$	$\frac{3}{16}\frac{(Uj)^2(Vk)\ (Wl)}{(\lambda k^2)\ (\lambda l^2)^2}$
minant term in Im p		$\pm\frac{1}{\sqrt{2}}\frac{(Uj)\ (Vk)\ (Wl)}{(\lambda k^2)\ (\lambda l^2)}$	$-\frac{(Uj)\ (Vk)\ (Wl)}{(\lambda k^2)\ (\lambda l^2)}$	—
lization of inequalities				
λk^2 λl^2		X^{-7} 1 X^6	X^{-9} 1 X^3	X^{-6} 1 X^6
Vk Wl		X^{-4} X^2 X^5	X^{-2} 1 X^2	1 X^2 X^5
p Im p		$\frac{1}{2}X^{-6}$ $\pm\frac{1}{\sqrt{2}}X^{-3}$	$\frac{7}{8}X^{-8}$ $-X^{-3}$	$\frac{3}{16}X^{-5}$ 0

Thus all successive components generated according to equation (11.11) from a field component satisfying equation (13.7) also satisfy equation (13.7). This is the required result. It also implies the cancellation of contributions to ϕ_{qr} in equation (11.13) involving no x-convection interaction steps. Equation (13.7) implies that the corresponding Fourier component of $\nabla \cdot \boldsymbol{H}$ is zero, and the result (13.8) is related through equations (8.9) and (8.6) to the vanishing of the divergence of the right-hand side of equation (8.3) when x-convection is ignored and $\nabla \cdot \boldsymbol{H}$ is zero.

The inequalities required for the convergence of the series (11.10), (11.12) or (11.13) for the three motions are shown, with the interaction step sequences which lead to them, in table 8. Those which apply to all the motions are in the first column. It is fairly easy to show for each motion that these conditions are sufficient, and imply that for different interaction step sequences the products of the factors involved are also much less than unity.

These inequalities also imply the rapid convergence of the iteration (11.9) for the eigenvalue p^*. The tensor ϕ_{qr} in equation (11.5) is itself a nonlinear function of p^*, and the conditions (11.8) were shown to be sufficient for the rapid convergence of the iteration. Now the eigenvalues of the tensor ϕ_{qr} in its most general form (12.1) are

$$\phi = \kappa \pm \sqrt{(\mu\nu)}. \tag{13.9}$$

From equation (11.13), the sequences of interaction steps contributing to the terms $\kappa/\lambda k^2$ and $\mu\nu/(\lambda k^2)^2$ are precisely of the form of the sequences of interaction steps mentioned above after equation (13.5); since they start and finish at $f_{0,0}$ or at $g_{0,0}$, and the number of factors λk^2 in the denominator is right. The corresponding contributions are therefore much less than one. So

$$\phi \ll \lambda k^2. \tag{13.10}$$

Similarly, differentiating equation (13.9), and the denominators in equation (11.13) for the terms $\kappa/\lambda k^2$ and $\mu\nu/(\lambda k^2)^2$, with respect to p^*,

$$\left|\frac{\mathrm{d}\phi}{\mathrm{d}p^*}\right| \ll 1,$$

where use has been made of the result,

$$\begin{aligned}\left|\frac{\mathrm{d}}{\mathrm{d}p^*}\{p^* + m^2(\lambda k^2) + n^2(\lambda l^2)\}^{-1}\right| &= |-\{p^* + m^2(\lambda k^2) + n^2(\lambda l^2)\}^{-2}| \\ &\leqslant \frac{3}{\lambda k^2}|\{p^* + m^2(\lambda k^2) + n^2(\lambda l^2)\}^{-1}|,\end{aligned}$$

which follows from equations (13.1) and (13.2) for m and n not both zero. Thus the conditions of equation (11.8) are satisfied, with c equal to $\frac{1}{2}\lambda k^2$, cf. equation (13.2).

Table 8 shows all the contributions to the tensor ϕ_{qr} which may be dominant with the conditions already applied. One typical closed interaction step sequence is shown for each contribution, with the total contribution and the total number of similar closed interaction step sequences, obtained from that shown by reflexions and possibly by putting the interaction steps in a different order. Sequences going from an $f_{0,n}$ or $g_{m,0}$ component to a $g_{0,n}$ or $f_{m,0}$ component without including any x-convections are ignored, from equation (13.8), and the restrictions shown in table 7 on page 442 are also applied. The denominators in equation (11.13) are represented by their dominant terms, using equations (11.8), (11.9) and (13.1), so that

$$\left.\begin{aligned}\{p^* + m^2(\lambda k^2) + n^2(\lambda l^2)\}^{-1} &\doteq \{n^2(\lambda l^2)\}^{-1} \quad \text{for} \quad n \neq 0, \\ &\doteq \{m^2(\lambda k^2)\}^{-1} \quad \text{for} \quad n = 0.\end{aligned}\right\} \tag{13.11}$$

This is a good approximation. However, if p^* is dominated by its imaginary part, its real part may be inaccurate if equation (13.11) is used. This was pointed out after the description of the iteration (11.9). The approximation,

$$\left.\begin{aligned}\{p^*+m^2(\lambda k^2)+n^2(\lambda l^2)\}^{-1} &\simeq \{n^2(\lambda l^2)\}^{-1} \quad \text{for} \quad n \neq 0,\\ &\simeq \{m^2(\lambda k^2)\}^{-1}\left\{1-\frac{\mathrm{i}\,\mathrm{Im}\,p^*}{m^2(\lambda k^2)}\right\} \quad \text{for} \quad n=0\end{aligned}\right\} \tag{13.12}$$

is sufficient in obtaining the dominant terms in ϕ_{qr} and in p^* for the motions considered here.

The next stage is to apply the iteration (11.9) to obtain the eigenvalue p^*, and to establish further conditions for the three motions so that its real part is positive. With the final condition that λj^2 is much less than $\mathrm{Re}\,p^*$, dynamo action is assured. For all three motions there is a negative contribution to κ from two x-convection steps, the x-component of the motion accelerates the natural diffusion decay rate λj^2. The extra conditions for growth shown in table 8 ensure that the regenerative terms are sufficient to overcome this. The analysis is easiest for the fourth motion, with ϕ_{qr} diagonal and with real equations. For the third motion ϕ_{qr} is complex diagonal, and the difficulty is greatest for the second motion.

For the fourth motion the regenerative term in $\kappa = p^*$, and the extra condition for it to be dominant, are shown in the table, with the result for the growth rate. It may be seen that dynamo action requires that the product $(Vk)\,(Wl)$ is positive; if this product is negative the inequalities already assumed exclude dynamo action.

For the third motion there are two negative contributions and an imaginary contribution to $\kappa = p_1^*$, as shown in table 8. It appears at first that dynamo action is excluded. But if the imaginary contribution is larger in absolute magnitude than the other two, its change may be important when equation (13.12) is used instead of equation (13.11) for the denominators in equation (11.13). Clearly in terms of the iteration (11.9), the real and imaginary parts of p_1^* are dominated by the terms in the table. But from equation (13.12) the second contribution to $\kappa = p_2^*$ is

$$-\mathrm{i}\,\frac{(Uj)\,(Vk)\,(Wl)}{(\lambda k^2)\,(\lambda l^2)}\left\{1-\frac{\mathrm{i}\,\mathrm{Im}\,p_1^*}{(\lambda k^2)}\right\}, \tag{13.13}$$

and the added real term is

$$\frac{(\mathrm{Im}\,p_1^*)^2}{(\lambda k^2)} = \frac{(Uj)^2\,(Vk)^2\,(Wl)^2}{(\lambda k^2)^3\,(\lambda l^2)^2}. \tag{13.14}$$

Further steps of the rapidly converging iteration (11.9) do not affect the dominant terms. The additional inequality required for growth, and the resulting dominant terms in $\mathrm{Re}\,p$ and $\mathrm{Im}\,p$, are shown in the table. It is interesting that the motion is still a second-order dynamo even if the signs of U, V or W are changed.

For the second motion it will be assumed at first that the product $(Vk)\,(Wl)$ is positive, since if the product is negative the motion (6.4), with a change of origin, is a multiple-scale version of the first motion (5.1). Then the dominant contributions to κ are negative, and the contributions to μ and ν are imaginary and all have the same sign. Substituting in equation (13.8), p_1^* has the dominant terms,

$$p_1^* = -\frac{(Uj^2)}{2(\lambda k^2)}\left\{1+\frac{(Vk)\,(Wl)}{(\lambda k^2)\,(\lambda l^2)}\right\} \pm \mathrm{i}\sqrt{\left[\frac{(Uj)^2\,(Vk)\,(Wl)}{(\lambda k^2)\,(\lambda l^2)}\left\{1+\frac{(Vk)\,(Wl)}{2(\lambda k^2)\,(\lambda l^2)}\right\}\right]}. \tag{13.15}$$

Using the additional assumption

$$\frac{(Vk)\,(Wl)}{(\lambda k^2)\,(\lambda l^2)} \gg 1 \tag{13.16}$$

(cf. the condition for growth shown in the table), the dominant terms are

$$p_1^* = -\frac{1}{2}\frac{(Uj)^2(Vk)(Wl)}{(\lambda k^2)^2(\lambda l^2)} \pm \frac{\mathrm{i}}{\sqrt{2}}\frac{(Uj)(Vk)(Wl)}{(\lambda k^2)(\lambda l^2)}. \tag{13.17}$$

As with the third motion, the additional contribution to the real part of p_2^* when equation (13.12) is used is

$$\frac{(\mathrm{Im}\, p_1^*)^2}{(\lambda k^2)} = \frac{1}{2}\frac{(Uj)^2(Vk)^2(Wl)^2}{(\lambda k^2)^3(\lambda l^2)^2}, \tag{13.18}$$

and is dominant, with the inequality (13.16). Further steps of the iteration (11.9) do not affect the dominant terms in p^*, which are shown in the table.

It is interesting to study the case for the second motion where the product $(Vk)(Wl)$ is negative. If

$$\left|\frac{(Vk)(Wl)}{(\lambda k^2)(\lambda l^2)}\right| \ll 1,$$

equation (13.15) becomes $$p_1^* = \pm Uj\sqrt{\left|\frac{(Vk)(Wl)}{(\lambda k^2)(\lambda l^2)}\right| - \frac{(Uj)^2}{2(\lambda k^2)}},$$

and the motion-resistivity combination is a first-order dynamo, giving growing solutions for all sufficiently small j. However, if

$$\left|\frac{(Vk)(Wl)}{(\lambda k^2)(\lambda l^2)}\right| \gg 1,$$

the analysis of the previous paragraph and the results in table 8 apply, and there is dynamo action to second order in j if λj^2 is small enough.

The final stage of the analysis is to demonstrate that the inequalities are consistent by giving a one-parameter limit $X \to \infty$ in which they are satisfied. Thus if

$$Wl = X^5, \quad \lambda l^2 = X^6,$$

the inequality (13.5) is asymptotically satisfied in the limit. A particular realization of the inequalities, chosen so that the spectral radius (13.6) is of order X^{-1}, is given for each motion at the end of table 8. The results there for $\mathrm{Re}\, p$ and $\mathrm{Im}\, p$ are asymptotically valid as $X \to \infty$.

14. Significance of the results

It remains in this concluding section to discuss the relevance of these results to further work on the dynamo problem.

Cowling (1933) proved that axisymmetric magnetic fields and fields independent of one Cartesian coordinate cannot be amplified or maintained by magnetohydrodynamic dynamo action. It has been shown by analytic counter-examples that the further statement that a motion independent of one Cartesian coordinate cannot give dynamo action is false.

Numerical results demonstrating dynamo action with convincing convergence have been obtained by making use of three devices. The first is the use of motions independent of the Cartesian coordinate x, so that in the eigenvalue equation (2.14) the eigenfunction $\boldsymbol{H}$ is a function of only the coordinates y and z, and its accurate numerical representation requires fewer variables than a function of all three Cartesian coordinates would require. The second is the removal of boundaries, so that the free decay rate $-\lambda j^2$ can be arbitrarily small; the natural decay rate for an insulated sphere of radius R is $-\pi^2\lambda/R^2$, and the rapid motions required to overcome this by

dynamo action imply large magnetic Reynolds numbers and extra convergence difficulties. The third device is the introduction in § 10 *b* of an eigenvalue method which does not involve the storage of the whole matrix and which is very fast. Time-stepping equation (2.10) would have involved even less storage, but much more time would be required to get an accurate growth rate.

Not all of these three devices are essential for convergence. Indeed in the earliest computations the eigenvalue method used the whole matrix. Further, the three-dimensional motion,

$$\boldsymbol{u} = (\cos y + \sin z,\ \cos z + \sin x,\ \cos x + \sin y), \tag{14.1}$$

is a first-order dynamo for at least almost all resistivities; the accurate growth rates could be found easily by the method of this paper, making use of the symmetry, for resistivities λ down to say $\frac{1}{2}$ or $\frac{1}{4}$. So the first device is not necessary. And it has now been established numerically that a steady axisymmetric motion $\boldsymbol{u}(r, \theta)$, chosen to be analogous to the first motion (5.1), can maintain and amplify indefinitely a non-axisymmetric magnetic field in an insulated sphere (Roberts 1972 *a*). So if the other devices are used the second is not essential.

The results of this paper are relevant to the dynamo action of turbulence, as studied by Steenbeck & Krause (1966, 1969); Steenbeck, Krause & Rädler (1966), Krause & Steenbeck (1967), Rädler (1969 *a*, *b*) and Moffatt (1970 *a*, *b*). They have analysed the dependence of the mean electromotive force $\overline{(\boldsymbol{v}' \times \boldsymbol{B}')}$ on $\bar{\boldsymbol{B}}$ and its derivatives, with isotropic turbulence and where there are preferred directions, using symmetry arguments, and for large resistivities λ using analysis comparable to that in §§ 3, I,5 and I,appendix A. If the turbulence is influenced by rotational motion with angular velocity $\boldsymbol{\Omega}$, and has a preferred direction $\boldsymbol{l}$, then

$$\overline{\boldsymbol{v}' \times \boldsymbol{B}'} = -\hat{\alpha}(\boldsymbol{\Omega} \cdot \boldsymbol{l})\bar{\boldsymbol{B}} + \hat{\beta}(\boldsymbol{l} \times \bar{\boldsymbol{B}}) - \hat{\gamma}(\nabla \times \bar{\boldsymbol{B}}) + \ldots, \tag{14.2}$$

where $\hat{\alpha}$, $\hat{\beta}$ and $\hat{\gamma}$ are scalars; the first term represents the isotropic symmetric part of the tensor α_{rs}, and the second term the antisymmetric part, cf. equation (3.2). Thus the first term leads to first-order dynamo action, the second to a phase velocity $\hat{\beta}\boldsymbol{l}$ of the growing magnetic field, and the third, with $\hat{\gamma}$ positive, implies enhanced diffusion. These effects are present with the illustrative motions considered here.

Finally, the numerical results apparently provide an approach to the detailed study of dynamo action at very small resistivities λ, that is, at large magnetic Reynolds numbers. Weiss (1966) demonstrated numerically that for small resistivities steady two-dimensional cellular motions will distort a uniform magnetic field so that the magnetic flux is concentrated at the edges of the cells in thin ropes. This flux concentration effect is likely to occur in a modified form in three-dimensional situations as well, and is probably important in stars, where the resistivity is very small. The dynamo models of Braginskii (1964 *a*, *b*) involve large magnetic Reynolds numbers, but since the motions are dominated by their axisymmetric toroidal part, ropes of magnetic flux do not arise. No attempt has been made here to show the form of the field eigensolutions, but for small resistivities they do have rope structure. With $j = 0$ the x-component of the motion can be neglected in finding the y- and z-components of the magnetic field. But the y- and z-components of the motion represent a cellular two-dimensional flow, with stream function $\cos y - \cos z$ for the first three motions, and $\frac{1}{2}(\cos 2y - \cos 2z)$ for the fourth, cf. figures 1 to 4. Thus flux ropes arise as in Weiss's calculations. In a future paper (Roberts 1972 *b*) it will be shown that the ropes have a thickness of order $\lambda^{\frac{1}{2}}$ as λ tends to zero, and for the first motion (5.1) the asymptotic behaviour of the function $a(\lambda)$ in equation (5.5) will be studied, and compared with table 3.

Appendixes

A. *Symmetry arguments for the Fourier-analysed equations*

Table 2 on page 428 shows the symmetry properties of the eigensolutions $\boldsymbol{h}_{m,n}$, and of their truncated approximations $\boldsymbol{h}^{(s)}_{m,n}$ (cf. equations (10.1) and (10.2)), which were used in the numerical work to reduce the number of independent Fourier components. Operations on the Fourier components which generate a new eigensolution from a given eigensolution are found, and it is shown that it is sufficient to confine attention to eigensolutions invariant under certain such operations, as indicated in the table.

The heuristic arguments in § 7 suggested that the dominant eigenvalues p are respectively real, complex in conjugate pairs, complex with negative imaginary part, and real, for the four motions, so that the field pattern is stationary only for the first and fourth motions.For eigensolutions with $\boldsymbol{h}^{\mathrm{A}}$ non-zero, this is confirmed analytically by study of the 2×2 tensor ϕ_{qr}, which has the respective shapes,

$$\begin{bmatrix} \kappa & \mu \\ -\mu & \kappa \end{bmatrix}, \quad \begin{bmatrix} \kappa & \mu \\ \mu & \kappa \end{bmatrix}, \quad \begin{bmatrix} \kappa & 0 \\ 0 & \kappa \end{bmatrix}, \quad \begin{bmatrix} \kappa & 0 \\ 0 & \kappa \end{bmatrix}.$$

These follow from the arguments of § 12, extended to general resistivities in appendix B, cf. equations (12.1) to (12.3). For the equality of the off-diagonal terms in the first two tensors (with a change of sign for the first), it is necessary to consider the additional one-to-one correspondence between closed interaction step sequences contributing in equation (11. 13) to the tensor ϕ_{qr}, obtained by exchanging f and g components and m and n suffices. Alternatively these two results follow from symmetry arguments like that of § 4. From equation (11.5), the eigenvalues p^* of these tensors are respectively

$$\kappa \pm \mathrm{i}\mu, \quad \kappa \pm \mu, \quad \kappa \quad \text{twice}, \quad \kappa \quad \text{twice},$$

for the four motions. Assume p^* is real. Then from equation (11.13) and from table 7 on page 442, the diagonal terms κ are complex only for the third motion; the terms μ are pure imaginary. So real eigenvalues can be expected only for the first and fourth motions. This is consistent with the heuristic arguments in § 7, summarized in table 1 on page 426. Even for the first and fourth motions complex eigenvalues can occur in conjugate pairs, but the dominant eigenvalues found were always real.

Suppose $\boldsymbol{h}$ is a solution of the equation (8.13) for the first motion, with components $(f_{m,n}, g_{m,n})$. Then so is $T\boldsymbol{h}$, with components

$$(T\boldsymbol{h})_{m,n} = (-1)^{m+n}(-g_{-n,m}, \quad f_{-n,m}). \tag{A 1}$$

Clearly,

$$\left.\begin{aligned} (T^2\boldsymbol{h})_{m,n} &= -(f_{-m,-n}, \quad g_{-m,-n}) = -\boldsymbol{h}_{-m,-n} \\ &= -(R\boldsymbol{h})_{m,n}, \end{aligned}\right\} \tag{A 2}$$

where R is the obvious operator which reflects the components about the origin. Thus defining I as the identity operator on solutions, and P_ω as

$$P_\omega = I + \omega T + \omega^2 T^2 + \omega^3 T^3, \tag{A 3}$$

where ω is 1 or -1 or i or $-\mathrm{i}$, it follows that

$$T^4 = R^2 = I, \tag{A 4}$$

$$(I - \omega T) P_\omega = I - \omega^4 T^4 = 0. \tag{A 5}$$

Thus $P_\omega \boldsymbol{h}$ is also an eigensolution (or possibly zero), and is invariant under ωT; and

$$4\boldsymbol{h} = \sum_\omega P_\omega \boldsymbol{h}. \tag{A 6}$$

Thus any eigensolution can be expressed as a sum of at most four eigensolutions, invariant under $\pm T$ or $\pm \mathrm{i}T$. So it is sufficient to confine attention to eigensolutions invariant under $\pm T$ or under $\pm \mathrm{i}T$.

For real eigenvalues, $\bar{Q}\boldsymbol{h}$ is also a solution, with components

$$(\bar{Q}\boldsymbol{h})_{m,n} = (\overline{g_{n,m}},\ \overline{f_{n,m}}), \tag{A 7}$$

and it is easy to show that

$$\bar{Q}^2 = I, \quad \bar{Q}(c\boldsymbol{h}) = \bar{c}(\bar{Q}\boldsymbol{h}), \quad \bar{Q}R = R\bar{Q}, \quad \bar{Q}T = T^3\bar{Q}.$$

Thus

$$\bar{Q}P_\omega = (I + \bar{\omega}T^3 + \bar{\omega}^2T^2 + \bar{\omega}^3T)\bar{Q} = P_\omega\bar{Q}. \tag{A 8}$$

So the eight sets of components $(I \pm \bar{Q})P_\omega \boldsymbol{h}$ are either zero or also eigensolutions, their sum is $8\boldsymbol{h}$, and they are invariant under $\pm\bar{Q}$ and under ωT. Further, if $\boldsymbol{h}$ is invariant under ωT and $\bar{Q}$, then $\mathrm{i}\boldsymbol{h}$ is invariant under ωT and under $-\bar{Q}$. So it is sufficient to confine attention to eigensolutions invariant under ωT and $\bar{Q}$.

Finally, if a solution is invariant under $\pm T$, it changes sign under R, and therefore $\boldsymbol{h}_{0,0}$ is zero. In the numerical work attention was confined to solutions with $\boldsymbol{h}_{0,0}$ non-zero, in agreement with the heuristic arguments in § 7. Further, these heuristic arguments suggest that $\boldsymbol{h}_{0,0}$ is a multiple of $(1, -\mathrm{i})$, so that $\mathrm{Re}\,(\boldsymbol{h}_{0,0}\,\mathrm{e}^{\mathrm{i}jx}) = (\cos jx, \sin hx)$, cf. table 1. Thus $g_{0,0} = -\mathrm{i}f_{0,0}$, and this suggests that the dominant solutions will be invariant under $-\mathrm{i}T$. This was confirmed numerically; solutions invariant under $\bar{Q}$ and under $\pm\mathrm{i}T$ were actually studied, and those invariant under $-\mathrm{i}T$ always gave larger growth rates.

The operations corresponding to equations (A 1) and (A 7), and generating new eigensolutions from given eigensolutions for the other three single-scale motions (6.1) to (6.3), are shown in table 2 on page 428. For the second motion the eigenvector $\bar{P}\boldsymbol{h}$ corresponds to the complex conjugate eigenvalue. For the second and third motions the reflexion operator R generates a new eigenvector, and commutes with all the other operators, cf. equation (A 8). For all three the operator Q generates a new eigensolution; this is because of the symmetry of the motions (6.1) to (6.3) between the y- and z-directions. The relevant properties of the operators are also shown in the table; they all have unit square, but they do not all commute.

For the fourth motion the two operators Q and S commute, and there is no difficulty. If s_Q and s_S are ± 1, and $\boldsymbol{h}$ is an eigenvector, then the four vectors $(I - s_Q Q)(I - s_S S)\boldsymbol{h}$ are either zero or eigenvectors invariant under $s_Q Q$ and $s_S S$, and their sum is $4\boldsymbol{h}$. The fact that each eigenvalue is repeated, the eigensolutions being degenerate, implies that it is sufficient to study eigensolutions invariant under Q. Eigensolutions invariant under $-S$ were ignored because of the assumption that $\boldsymbol{h}_{0,0}$ is non-zero.

For the second and third motions the situation is more complicated, since although the reflexion operator R commutes with the other operators, the operator Q does not commute with P or $\bar{P}$. As with the fourth motion it is possible to confine attention to eigensolutions $\boldsymbol{h}$ invariant under $s_R R$ and $s_Q Q$. Then, from the results in the table, $\bar{P}\boldsymbol{h}$ for the second motion and $P\boldsymbol{h}$ for the third are invariant under $s_R R$ and $-s_R s_Q Q$. Unless s_R is unity $h_{0,0}$ is zero. So for the second motion attention was largely confined to eigensolutions invariant under R and Q; the numerical work confirmed that solutions invariant under R and $-Q$ have the complex conjugate eigenvalues.

For the third motion, if the eigensolution $\boldsymbol{h}$ is invariant under R and Q, then $P\boldsymbol{h}$ and $(I-s_pP)\boldsymbol{h}$ are non-zero eigenvectors and are respectively invariant under $-Q$ and s_pP. Clearly the eigenvalues are repeated, attention can be confined to eigensolutions invariant under R and Q or under R and P. The possible symmetry properties for solutions invariant under $-R$ are shown in the table.

B. *The shape of the tensor* ϕ_{qr}

In this appendix the results (12.1), (12.2) and (12.3), for the shape of the tensor ϕ_{qr} introduced in § 11, are extended to cases where the series (11.10), and (11.12) for $\boldsymbol{h}'$, and (11.13) for ϕ_{qr}, do not converge. The extension is relevant to this paper only in the verification of the accuracy of the computer programs for the multiple-scale versions of the third and fourth motions by their giving degenerate eigenvalues in all cases, as predicted by equations (12.2) and (12.3). But the result and the method of proof are interesting in themselves.

The results (12.1) to (12.3) were established from equation (11.13) by showing that for each value of ω the total contribution to the tensor ϕ_{qr} has the given shape. Now the equation (11.4) determining $\boldsymbol{h}'$ in terms of $\boldsymbol{h}^{\mathrm{A}}$ can be written as

$$(\mathscr{I}-\mathscr{Q})\boldsymbol{h}' = \{p^* + m^2(\lambda k^2) + n^2(\lambda l^2)\}^{-1}\mathscr{U}'^{\mathrm{A}}\boldsymbol{h}^{\mathrm{A}}, \tag{B 1}$$

where $\mathscr{I}$ is the identity operator and

$$\mathscr{Q}\boldsymbol{h}' = \{p^* + m^2(\lambda k^2) + n^2(\lambda l^2)\}^{-1}\mathscr{U}''\boldsymbol{h}' \tag{B 2}$$

cf. equations (13.6), (11.11), (3.3), (3.4) and (3.5). If the sequence,

$$P_N(\mathscr{Q}) = \sum_0^N \mathscr{Q}^n, \tag{B 3}$$

is uniformly convergent, then the limit is the unique inverse $(\mathscr{I}-\mathscr{Q})^{-1}$. So equation (B 1) has the solution given by equations (11.10) and (11.11), and the result (11.13) and its consequences (12.1) to (12.3) apply. However, for these consequences it is sufficient that there is an alternative sequence of polynomials $P_N(\mathscr{Q})$ converging uniformly to the inverse $(\mathscr{I}-\mathscr{Q})^{-1}$, since the contribution to ϕ_{qr} from any power of $\mathscr{Q}$ has the required shape. The contribution from $\mathscr{Q}^n$ is the term in (11.13) with ω equal to $n+2$.

Now the operator $\mathscr{Q}$ is compact, because it is the uniform limit of a sequence of operators with finite dimensional range (see § I, appendix B; in effect, this just means that whatever the values of p^*, λk^2, λl^2, Uj, Vk and Wl are, the term $\{p^* + m^2(\lambda k^2) + n^2(\lambda l^2)\}$ is much greater than the terms of $\mathscr{U}''$ for sufficiently large values of $|m| + |n|$). Thus $\mathscr{Q}$ has a bounded spectrum of discrete eigenvalues in the complex plane, with no point of accumulation except possibly zero (Dunford & Schwartz 1958, p. 579). There are therefore only a finite number of eigenvalues $q_1, \ldots, q_n$ with $|q_i| \geqslant 1$; the remainder of the spectrum satisfies $|q| < 1-2\epsilon$ for some positive ϵ, and from the assumption that $(\mathscr{I}-\mathscr{Q})^{-1}$ exists, $q_i \neq 1$ for any i. The resolvent $(q\mathscr{I}-\mathscr{Q})^{-1}$ is defined and analytic in q on the resolvent set, the complement of the spectrum, and has poles of finite order ν_i at the eigenvalues q_i.

Now consider the problem of approximating the function $(1-x)^{-1}$ by polynomials. Let

$$M = \sum_{i=1}^{n} \nu_i$$

and define

$$\left.\begin{aligned} y_0 &= \sum_{j=0}^{N-M} x^j, \\ y_m &= y_{m-1} + \alpha_m\{1-(1-x)\,y_{m-1}\}, \quad m = 1, 2, \ldots, M, \\ P_N(x) &= y_m. \end{aligned}\right\} \tag{B 4}$$

Then the error $f_m = y_m - (1-x)^{-1}$ satisfies the equations

$$f_0 = x^{N-M+1}/(x-1),$$
$$f_m = f_{m-1}\{1-\alpha_m(1-x)\},$$

and the error $e_N(x)$ of $P_N(x)$ is

$$\begin{aligned} e_N(x) &\equiv P_N(x) - (1-x)^{-1} \\ &= \frac{x^{N-M+1}}{x-1} \prod_1^M \{1-\alpha_m(1-x)\}. \end{aligned} \tag{B 5}$$

Now define

$$\left.\begin{aligned} \alpha_i &= \frac{1}{1-q_1} \quad (i = 1, 2, \ldots, \nu_1), \\ \alpha_i &= \frac{1}{1-q_2} \quad (i = \nu_1+1, \nu_1+2, \ldots, \nu_1+\nu_2), \end{aligned}\right\} \tag{B 6}$$

and so on. Then the error $e_N(x)$ tends uniformly to zero for $|x| \leqslant 1-\epsilon$, and has a zero of order ν_i at the eigenvalues q_i of $\mathscr{Q}$ satisfying $|q_i| \geqslant 1$.

It can now be proved that

$$e_N(\mathscr{Q}) \equiv P_N(\mathscr{Q}) - (\mathscr{I} - \mathscr{Q})^{-1} \to 0, \tag{B 7}$$

uniformly, as $N \to \infty$. For (Dunford & Schwarz 1958, p. 568)

$$e_N(\mathscr{Q}) = \frac{1}{2\pi i}\int_{\Gamma_1} \frac{e_N(q)\,dq}{q\mathscr{I} - \mathscr{Q}} + \frac{1}{2\pi i}\int_{\Gamma_2} \frac{e_N(q)\,dq}{q\mathscr{I} - \mathscr{Q}}, \tag{B 8}$$

where Γ_1 is the positively oriented circle with centre the origin and radius $1-\epsilon$, and Γ_2 is a Jordan curve enclosing the spectral points $q_1, q_2, \ldots, q_n$ in a positive sense, lying strictly outside the circle Γ_1, and with the point $q = 1$ outside it. Now the integrand is analytic on and within Γ_2, since the resolvent $(q\mathscr{I} - \mathscr{Q})^{-1}$ has a pole of order ν_1 and the function $e_N(q)$ has a zero of order ν_i at the value $q = q_i$. So the integral round Γ_2 vanishes, by Cauchy's theorem. Further, on Γ_1 the resolvent is bounded and $e_N(q)$ tends uniformly to zero. The result (B 7) follows. Thus if the tensor ϕ_{qr} exists it takes the shapes (12.1), (12.2) and (12.3) respectively, for the three motions (6.4), (6.5) and (6.6), whether equation (11.13) is convergent or not.

C. *Accuracy of the computer programs*

The equations (8.10) to (8.13) which have been solved are quite lengthy and complicated, and so is the detailed application of the symmetry conditions shown in table 2 on page 428. It is therefore important to demonstrate that the computer programs do indeed represent the equations correctly, without forcing the reader to make a detailed examination of each one.

The accuracy of the programs for the four motions is confirmed by the agreement of the numerical results with the respective analytic results,

$$p = \frac{j}{\lambda} - \lambda j^2 - \frac{j^2}{\lambda} + O\left(\frac{j}{\lambda^3}\right), \tag{C 1}$$

$$p = \pm \mathrm{i}\left\{\frac{j}{\lambda} + O\left(\frac{j}{\lambda^3}\right)\right\} - \lambda j^2 - \frac{j^2}{\lambda} + O\left(\frac{j^2}{\lambda^3}\right), \tag{C 2}$$

$$p = -\mathrm{i}\left\{\frac{3j}{4\lambda^2} + O\left(\frac{j}{\lambda^4}\right)\right\} - \lambda j^2 - \frac{j^2}{2\lambda} + O\left(\frac{j^2}{\lambda^3}\right), \tag{C 3}$$

$$p = -\lambda j^2 - \frac{j^2}{4\lambda} + O\left(\frac{j^2}{\lambda^3}\right), \tag{C 4}$$

which are valid for $\lambda \gg 1$ and $j \leqslant 1$. These results follow from analysis similar to the multiple-scale analysis of § 13, but with

$$U = V = W = k = l = 1, \tag{C 5}$$

so that equation (13.1) and its consequences do not apply. The regenerative terms are of order j^2/λ^5 for the second and third motions, and of order j^2/λ^3 for the fourth, but with equations (C 5) holding and with $\lambda \gg 1$ the many negative contributions swamp them.

The accuracy of the two programs for the first motion, the second assuming a real eigenvalue and making use of an additional symmetry property, is further confirmed by their exact agreement together, and by their giving real eigenvalues (despite the matrix being complex and non-Hermitian so that any error in the program would be likely to remove this property).

The accuracy of the program for the second motion is confirmed by the agreement of the numerical results with the result of appendix A, shown in table 2, that if $\{p, \boldsymbol{h}^{(s)}_{m,n}\}$ is an eigensolution with $\boldsymbol{h}_{m,n}$ invariant under R and Q, then $\{\bar{p}, (\bar{P}\boldsymbol{h})^{(s)}_{m,n}\}$ is an eigensolution invariant under R and $-Q$.

The accuracy of the programs for the third and fourth motions is further confirmed by results obtained with separate multiple-scale programs, the truncation equation (10.1) being used for both motions, and fewer symmetry conditions. The application of these programs for various realizations of the inequalities of § 13 and table 8 and for $s \geqslant 2$ gave numerical results in precise agreement with the analytic ones; the application with equation (10.26) holding (and with s sufficiently large for the fourth motion with a different truncation) gave results agreeing with those for the single-scale computer programs. Further, the identical degeneracy of the eigenvalues indicated by the tensor shapes (12.2) and (12.3), and shown to apply generally in appendix B, was confirmed by the numerical results obtained using the multiple-scale programs. Eigensolutions with $f_{0,0}$ zero and with $g_{0,0}$ zero had eigenvalues agreeing to 12 significant figures.

The author wishes to thank his research supervisor, Dr H. K. Moffatt, for his help and encouragement during this work. The Science Research Council supported the early stages with a Research Studentship at the Department of Applied Mathematics and Theoretical Physics, University of Cambridge. It was completed at the Department of Applied Mathematics, University of Newcastle upon Tyne, while the author was working with Professor P. H. Roberts as a Senior Research Associate, with the research grant GR/3/425 from the Natural Environment Research Council. The computations were done on 'Titan' in the Cambridge University Mathematical Laboratory during 1967, and grateful acknowledgement is made to the Director and staff for making the machine available and for help given.

PHILOSOPHICAL TRANSACTIONS OF THE ROYAL SOCIETY A MATHEMATICAL, PHYSICAL & ENGINEERING SCIENCES

References

Braginskii, S. I. 1964*a* *J. exp. theor. Phys.* **47**, 1084 (*Soviet Phys. JETP* **20**, 726).

Braginskii, S. I. 1964*b* *J. exp. theor. Phys.* **47**, 2178. (*Soviet Phys. JETP* **20**, 1462).

Bullard, E. C. & Gellman, H. 1954 *Phil. Trans. R. Soc. Lond.* A **247**, 213.

Childress, S. 1967 Report AFOSR-67-0124, Courant Institute, New York.

Cowling, T. G. 1933 *Mon. Not. R. astr. Soc.* **94**, 39.

Dunford, N. & Schwartz, J. T. 1958 *Linear operators. I. General theory*. New York: Interscience.

Gibson, R. D. & Roberts, P. H. 1969 The Bullard-Gellman dynamo, p. 577. In *The application of modern physics to the earth and planetary interiors* (*Proc. NATO Adv. Study Inst., Newcastle*, April 1967, ed. by S. K. Runcorn). London: Wiley–Interscience.

Krause, F. & Steenbeck, M. 1967 *Z. Naturf.* **22***a*, 671.

Lilley, F. E. M. 1970 *Proc. R. Soc. Lond.* A **316**, 153.

Moffatt, H. K. 1970*a* *J. Fluid Mech.* **41**, 435.

Moffatt, H. K. 1970*b* *J. Fluid Mech.* **44**, 705.

Rädler, K.-H. 1969*a* *Mber. dt. Akad. Wiss.* **11**, 194.

Rädler, H.-K. 1969*b* *Mber. dt. Akad. Wiss.* **11**, 272.

Roberts, G. O. 1969 Dynamo waves, p. 603. In *The application of modern physics to the Earth and planetary interiors* (*Proc. NATO Adv. Study Inst., Newcastle*, April 1967, ed. by S. K. Runcorn). London: Wiley–Interscience.

Roberts, G. O. 1970*a* *Phil. Trans. R. Soc. Lond.* A **266**, 535.

Roberts, G. O. 1970*b* Ph.D. dissertation, University Library, Cambridge.

Roberts, G. O. 1972*a* *Numerical results on the dynamo action of axisymmetric motions in a sphere*. To appear.

Roberts, G. O. 1972*b* *Flux expulsion and dynamo action at large magnetic Reynolds numbers*. To appear.

Steenbeck, M. & Krause, F. 1966 *Z. Naturf.* **21***a*, 1285.

Steenbeck, M. & Krause, F. 1969 *Astr. Nachr.* **291**, 49.

Steenbeck, M., Krause, F. & Rädler, K.-H. 1966 *Z. Naturf.* **21***a*, 369.

Weiss, N. O. 1966 *Proc. R. Soc. Lond.* A **293**, 310.

Wilkinson, J. H. 1965 *The algebraic eigenvalue problem*. Oxford: Clarendon Press.

PHILOSOPHICAL TRANSACTIONS OF THE ROYAL SOCIETY A MATHEMATICAL, PHYSICAL & ENGINEERING SCIENCES